Bull Volcanol (2015) 77:47
DOI 10.1007/s00445-015-0916-0

RESEARCH ARTICLE

Effects of deglaciation on the petrology and eruptive history of the Western Volcanic Zone, Iceland

Deborah E. Eason[1] · **John M. Sinton**[1] · **Karl Grönvold**[2] · **Mark D. Kurz**[3]

Received: 3 October 2012 / Accepted: 14 March 2015

Abstract New observations and geochemical analyses of volcanic features in the 170-km-long Western Volcanic Zone (WVZ) of Iceland constrain spatial and temporal variations in volcanic production and composition associated with the last major deglaciation. Subglacial eruptions represent a significant portion of the late Quaternary volcanic budget in Iceland. Individual features can have volumes up to ~48 km^3 and appear to be monogenetic. Subaqueous to subaerial transition zones provide minimum estimates of ice sheet thickness at the time of eruption, although water-magma interactions and fluctuating lake levels during eruption can lead to complex lithological sequences. New major and trace element data for 36 glacial and postglacial eruptive units, combined with observations of lava surface quality, passage zone heights, and ^{3}He exposure ages of some glacial units, indicate a maximum in volcanic production in the WVZ during the last major ice retreat. Anomalously high volcanic production rates continue into the early postglacial period and coincide with significant incompatible element depletions and slightly higher CaO and SiO_2 and lower FeO content at a given MgO. Subglacial units with strong incompatible element depletions also have lava surfaces that lack evidence of subsequent glaciation. These units likely formed after the onset of deglaciation, when rapidly melting ice sheets increased decompression rates in the underlying mantle, leading to anomalously high melting rates in the depleted upper mantle. This process also can explain the eruption of extremely depleted picritic lavas during the early postglacial period. These new observations indicate that the increased volcanic activity associated with glacial unloading peaked earlier than previously thought, before Iceland was completely ice free.

Keywords Subglacial volcanism · Iceland · Mid-ocean ridge · Igneous petrology · Mantle melting · Deglaciation

Editorial responsibility: T. Thordarson

Electronic supplementary material The online version of this article (doi:10.1007/s00445-015-0916-0) contains supplementary material, which is available to authorized users.

✉ Deborah E. Eason
deborahe@hawaii.edu

[1] Department of Geology and Geophysics, School of Ocean and Earth Science and Technology, University of Hawai'i at Mānoa, 1680 East-West Rd, Honolulu, HI 96822, USA

[2] Nordic Volcanological Center, University of Iceland, Askja, 101, Reykjavík, Iceland

[3] Department of Marine Chemistry and Geochemistry, Woods Hole Oceanographic Institution, Woods Hole, MA 02543, USA

Introduction

The end of the last major deglaciation was associated with unusually high volcanic productivity and correlated changes in lava composition throughout Iceland's neovolcanic zones. This phenomenon has been inferred for the Reykjanes Peninsula (Jakobsson et al. 1978; Gee et al. 1998), the Western Volcanic Zone (WVZ) (Sinton et al. 2005), Veiðivötn in the Eastern Volcanic Zone (Vilmundardóttir and Larsen 1986), and the Theistareykir and Krafla regions (Sæmundsson 1991; Slater et al. 1998; Maclennan et al. 2002) in the Northern Volcanic Zone (NVZ). Evidence suggests that magma production in the early postglacial period was up to ~30 times the present-day values and coincided with large changes in incompatible element content of the erupted lavas (e.g., Maclennan et al. 2002; Sinton et al. 2005). Although some authors relate the eruption pulse to enhanced tapping of crustal magma chambers in response to the mechanical effects of glacial unloading

Published online: 09 May 2015

(Gudmundsson 1986; Gee et al. 1998), theoretical considerations (Jull and McKenzie 1996) and chemical data (Hardarson and Fitton 1991; Slater et al. 1998; Maclennan et al. 2002; Sinton et al. 2005) are consistent with an increase in melting rates due to enhanced mantle decompression resulting from glacial unloading.

Prior studies have mainly looked at volcanic production only in the postglacial record or compared chemical variations in a small number of postglacial and glacial units. Thus, while correlations between ice removal and increased volcanic output are expected, the paucity of detailed data on late glacial volcanism limits our understanding of the detailed timing and magnitude of this effect (Licciardi et al. 2007; Jakobsson and Gudmundsson 2008). Since melt migration rates are finite, there should be a lag between the unloading-induced increase in mantle melting and the corresponding increase in volcanic production at the surface, but the magnitude of this effect is currently unconstrained by observation.

Within the WVZ, the postglacial record exhibits a peak in volcanic productivity and related geochemical variations in the first 2000 years following ice removal. However, the postglacial history records only the after-effects of deglaciation. Did even higher volcanic production characterize the late glacial period? Do late glacial eruptions show even stronger geochemical signatures of enhanced mantle melting? How soon after the onset of deglaciation and the resulting mantle melting perturbation are the effects seen on the surface?

The goal of this study was to examine a representative number of subglacial features within the WVZ with the objective of extending the eruptive chronology and associated geochemical variability into the last glacial period. We selected a suite of 20 subglacial edifices in the WVZ (Fig. 1) for this study. We have distinguished the subaqueously and subaerially formed lithologies that comprise each of these features, evaluated their eruptive conditions and erosional history, and estimated their total eruptive volumes. We report new geochemical data on these units, including glass and whole rock chemical analyses for major and trace elements, and four new cosmogenic ^{3}He exposure ages. In addition, we have refined the postglacial eruptive history of the WVZ reported in Sinton et al. (2005) with new constraints on the ages of several postglacial units and previously unreported trace element data. The combined data represent the most complete time-stratigraphic eruption record for any length of mid-ocean ridge and more fully document the magmatic response to deglaciation in western Iceland.

Effusive volcanism takes two primary forms: fissure eruptions and lava shields (central vent eruptions). In the subglacial environment, the products of fissure eruptions are tindars or móberg ridges, whereas lava shields commonly form tuyas or table mountains. In this study, we concentrate on the latter because they (1) tend to be larger in volume and therefore dominate the volcanic budget, (2) have passage zones that can be used to estimate ice thickness at the time of eruption, and (3) are surmounted by subaerial lava that is amenable to geological observations on posteruption erosion and exposure age dating.

Tuya morphology

Table mountains, also known as tuyas (Mathews 1947), or *stapi* in Icelandic (e.g., Kjartansson 1959), are the products of subglacial volcanic eruptions and have distinctive morphological characteristics derived from eruption through an ice sheet. Generally thought to be monogenetic, these steep-sided, nearly flat-topped features are the subglacial equivalent of lava shields and are common in Iceland (e.g., Kjartansson 1959; Walker 1965; Jones 1969, 1970; Skilling 2009), western Canada (e.g., Mathews 1947; Moore et al. 1995; Edwards et al. 2009), and Antarctica (e.g., Smellie et al. 1993; Smellie 2000). Interactions between the erupting lava and melting ice can lead to sudden changes in eruption style and produce complicated morphological features and lithological sequences (e.g., Smellie 2000; Werner and Schmincke 1999; Skilling 2009).

Subglacial eruptions initially produce steep-sided volcanic edifices composed of pillow lavas and hyaloclastite breccias in an ice-confined lake of glacial meltwater (e.g., Kjartansson 1961; Jones 1969, 1970; Smellie 2000). Once the eruptive vent emerges above the lake surface either from edifice growth or lake drainage, the eruption style changes to subaerial lava effusion, producing the capping, low-angle lava shield that gives these features their characteristic shape (Fig. 2). The contact between the subaerial capping lavas and the underlying subaqueous unit is known as the passage zone (Jones 1969). A single eruption can include multiple rounds of lake filling and draining, sometimes generating multiple passage zones (e.g., Jones 1969; Smellie 2006; Skilling 2009). The highest of these transitions marks the maximum known elevation of the ice-ponded lake and so provides a minimum estimate of ice thickness at the time of eruption (e.g., Walker 1965; Jones 1969; Sæmundsson 1980; Guðmundsson 1998; Werner and Schmincke 1999).

Not all subglacial eruptions emerge above the lake surface nor produce classic table mountain morphology. Elongate ridges of hyaloclastite and/or pillow lavas, sometimes called tindars or móberg ridges, are another form of subglacial eruption, interpreted to be the subglacial equivalents of fissure eruptions. Hyaloclastite ridges typically lack a subaerial lava sequence, but the relationship between them and tuyas is gradational and some units may have features spanning the two categories. Just as postglacial fissure eruptions in the WVZ tend to have lower eruptive volumes on average than lava shields (Sinton et al. 2005), móberg ridges tend to be smaller than tuyas (e.g., Jakobsson and Johnson 2012; Pederson and Grosse 2014).

Some WVZ units contain only localized and/or thin subaqueous sections of pillow lava, breccia, and/or hyaloclastite, suggesting limited ice or water interaction. These units did not

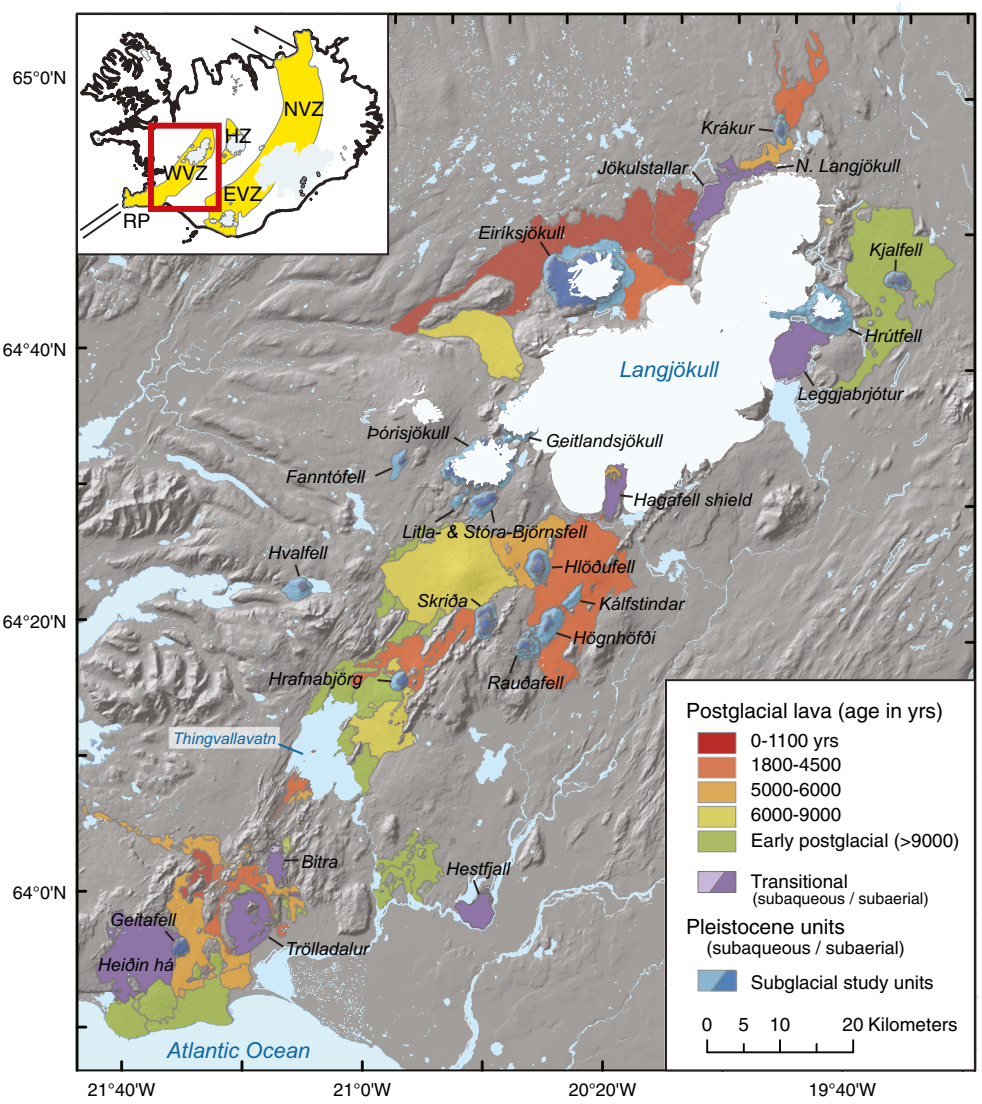

Fig. 1 Shaded relief map of the WVZ showing the distribution of postglacial, transitional, and subglacial eruptive units of this study (modified from Sæmundsson 1991; Jóhannesson and Sæmundsson 1998; Sinton et al. 2005; Sæmundsson et al. 2010). *Lighter* and *darker shades* of subglacial units denote subaqueous lithologies (pillow lavas and/or hyaloclastite) and subaerial lava flows, respectively. See Supplementary Material for maps of individual units. *Inset*: Map showing the principal plate-boundary zones in Iceland: the Reykjanes Peninsula (*RP*), Western Volcanic Zone (*WVZ*), Hofsjökull Zone (*HZ*), Eastern Volcanic Zone (*EVZ*), and Northern Volcanic Zone (*NVZ*)

erupt through an ice sheet sufficiently thick or extensive to build the classic table mountain morphology, and in some cases, it is not clear whether the water interaction was related to an ice sheet or something else (e.g., higher relative sea levels). We call these features transitional units in this paper, but many have previously been referred to as "finiglacial" (e.g., Sæmundsson 1995; Sinton et al. 2005) as they are thought to have formed near the end of the last glacial period when ice sheet extents were waning.

Tuyas can be extremely large, the biggest being Eiríksjökull in the WVZ with an estimated eruptive volume of ~48 km^3. These impressive features represent a significant portion of the volcanic budget in Iceland, but little documentation currently exists on them. Chemical data on Icelandic tuyas are relatively sparse; Moore and Calk (1991) presented glass and whole rock analyses from six tuyas, and Jakobsson and Johnson (2012) presented data from ~37 WVZ intraglacial units, including both tuyas and tindars. Eruption ages for subglacial features are extremely difficult to determine. Radiocarbon dating is impossible due to the lack of preserved organic material, and many are relatively young, low-K basalts, making them unsuitable candidates for radiometric dating by $^{40}Ar/^{39}Ar$ and K-Ar methods. Licciardi et al. (2007) applied cosmogenic exposure dating to selected table mountains and discussed the potential limitations of this chronologic tool for these unique volcanic features.

Cosmogenic ^{3}He analysis of six WVZ table mountains by Licciardi et al. (2007) all yielded late glacial ages, consistent with eruption through a thinning ice sheet, but not all tuyas are necessarily late glacial in age. Identifying which ones are part of this process and constraining their approximate eruption ages are important steps to understanding the interrelationships among glacial unloading, mantle melting, and volcanic output, and to exploiting this unique process to investigate fundamental aspects of mantle melting.

Fig. 2 Features of WVZ subglacial volcanic edifices. **a** Hrútfell exhibits classic tuya morphology with a single, roughly horizontal passage zone (*yellow dotted line*). **b** Multiple passage zones visible on the upper reaches of Hlöðufell. **c** Hestfjall's southward-dipping passage zone and summit scoria cone. **d** Scoria cone on Skriða coinciding with the passage zone. **e** Subaerial lava of Þórisjökull showing unmodified ropy pāhoehoe structure. **f** Contact relations showing Þórisjökull hyaloclastite overlying Geitlansjökull

Glacial chronology

Evidence from glacial moraines, radiocarbon ages on marine sediments, locations and elevations of marine terraces and strandlines, as well as other empirical data on climate and vegetation history have been used to construct the likely distribution of Icelandic glaciers from the last glacial maximum (LGM, ~25 ka) to present day (see Geirsdóttir et al. (2007, 2009), Norðdahl et al. (2008), and Le Breton et al. (2010) for reviews).

During the LGM, ice extended beyond the present shoreline with an estimated maximum ice sheet thickness of about 2000 m (Norðdahl and Pétursson 2005; Hubbard et al. 2006). Ice retreat began during the Oldest Dryas (~18–14.7 ka), culminating in a catastrophic breakup of the LGM ice sheet and rapid deglaciation during the Bølling-Allerød warm stage (~14.7–12.8 ka) which led to an estimated ~75 % reduction in the ice sheet size (Geirsdóttir and Eiríksson 1994; Geirsdóttir et al. 2000). This warming may have been interrupted by a brief cold snap during the Older Dryas stage (~14–13.7 ka), and a longer cold snap led to a readvancement of the ice sheet during the Younger Dryas (YD, ~12.8–11.7 ka, Fig. 6). Current estimates of the YD ice sheet suggest it reached <50 % the size of the LGM ice sheet, with significant portions of the southern lowlands remaining ice free (Geirsdóttir et al. 2007, 2009).

Beginning around ~11.7 ka (Pre-Boreal, ~11.7–10.5 ka), the ice sheet again went into retreat, and isostatic rebound caused sea level to fall below the present shoreline. By the onset of the Boreal stage (~10.5–8 ka), Iceland is thought to have been largely ice free, except for perhaps the highest peaks. Isostatic rebound, which lags behind glacial melting, probably was completed by ~9–8 ka (Sigmundsson 1991). Meanwhile, another significant cold snap occurred 8.2 ka ago and may have resulted in renewed growth of glaciers in the highlands around Langjökull. Iceland is thought to have been largely ice free during the mid-Holocene thermal optimum (Geirsdóttir et al. 2009; Larsen et al. 2012). The present-day glaciers began to form during the neoglaciation ~5 ka, and recent modeling suggests that Langjökull grew to encompass many of the surrounding peaks (e.g., Þórisjökull, Eiríksjökull, Geitlandsjökull, and Hrútfell), which may have hosted permanent snow cover or a passive glacier for most of the past ~2 kyr (Flowers et al. 2008).

Methods

Field study

This study focuses on 20 subglacial units selected for their youthful appearance (lack of extensive erosion, slumping, soil development), presence of capping subaerial lava, and accessibility. By focusing on tuyas rather than hyaloclastite ridges, this study assesses the eruptive characteristics of the volumetrically most important manifestations of subglacial activity in the WVZ.

Table 1 provides a summary of primary observations on tuyas in this study, with preliminary geologic maps, sample locations, and field observations of individual units available in Supplementary Materials. For each feature, we attempted to determine the general distribution of pillow lava, hyaloclastite breccia, and finer grained, well-bedded hyaloclastites within the subglacial sections; identify passage zone height(s); make observations of the extent of modification of subaerial lava surfaces; and collect samples at various stratigraphic levels for geochemical analysis. In most cases, this was accomplished in 1–3 days of field work on each feature. Our new mapping relies heavily on prior work by Sæmundsson (1992, 1995), Jóhannesson and Sæmundsson (1998), Sinton et al. (2005), and predecessors, with contacts located precisely in areas we visited (solid lines), and inferred based on topography and/or visual observations of areas we were unable to visit in the field (dashed lines). In several cases, we found internal contacts significant enough to merit further investigation into the unit's monogeneity (see later sections). For units with capping subaerial lava, we report passage zone heights (the passage zone elevation minus the average base elevation), which correspond to the minimum heights of the confined intraglacial lake levels at the time of emergence. Eruptive volumes were calculated in ArcGIS using a 50-m spatial resolution digital elevation model and an estimated base elevation for each individual eruptive unit, and are comparable with previous estimates (e.g., Moore and Calk 1991; Licciardi et al. 2007; Jakobsson and Johnson 2012).

Table 1 Tuyas and transitional units of the Western Volcanic Zone

Unit	Type	Volume (km^3)	Passage height (m)	Chemical group	Surface group	Exposure age (ka)[a]
Heiðin há	Transitional	6.8	–	A	I	9.3±0.4*
Jökulstallar	Transitional	8.1	140	A	I	
Leggjabrjótur	Transitional	6.3	80	A	I	
N. Langjökull	Transitional	5.3	160	A	I	
Hagafell shield	Transitional	4.5	160	A	I	
Trölladalur	Transitional	3.2	50	A	I	
Þórisjökull	Subglacial	10.7	300	A	I	11.6±0.3*
Eiríksjökull	Subglacial	48.2	540	A	II	
Krákur	Subglacial	0.8	240	A	II	
Kjalfell	Subglacial	0.8	330	A	II	9.9±0.6*
Bitra	Transitional	0.7	>260	B	II	
Hestfjall	Transitional	1.7	210	B	II	
Hlöðufell	Subglacial	3.9	460	B	II	(10.7**)
Skriða	Subglacial	3.4	320	B	II	10.5±0.2
Geitlandsjökull	Subglacial	5.2	480	B	III	
Stóra-Björnsfell	Subglacial	2.6	470	B	IV	7.1±0.2*
Geitafell	Subglacial	1.0	220	C	III	11.4±0.7
Hrafnabjörg	Subglacial	1.5	380	C	III	
Hvalfell	Subglacial	2.9	470	C	III	12.6±0.4
Litla-Björnsfell	Subglacial	0.4	>520	C	–	
Fanntófell	Subglacial	0.7	290	C	IV	
Högnhöfði	Subglacial	3.8	540	C	IV	10.2±0.3
Kálfstindar	Subglacial	1.1	>540	C	–	
Rauðafell	Subglacial	4.1	620	C	IV	12.2±0.2
Hrútfell	Subglacial	11.5	600	C	IV	

[a] Asterisk (*) denotes new ages from data presented in this study. All others from Licciardi et al. (2007), with (**) denoting a revised age for Hlöðufell based on a more recent unpublished analysis (Licciardi, personal communication). See text for definition of chemical groups and the assignment of individual edifices. Passage heights are heights above the base of the edifice

Observations of subaerial lava surfaces were used to assess the extent of modification by ice after eruption. For those units with relatively unmodified ropy pāhoehoe or other surface features, samples were collected for exposure age dating. Surface samples were collected in accordance with the methods described in Licciardi et al. (2007), targeting olivine-phyric surface lava from high-standing areas such as tumuli and other lava rises to minimize the possible effects of burial. Samples collected for whole rock geochemical analyses were taken from the fresher, massive interiors of subaerial lavas and pillows to minimize alteration. Where present, glassy rinds from pillows and scoria were collected for major element analysis by electron microprobe. We attempted to maximize spatial coverage while sampling the greatest vertical stratigraphic section possible within each unit in order to investigate their petrological evolution. Sample locations for individual units are shown on the geologic maps in the Supplementary Material.

Geochemical analyses

Major and trace element data were collected on whole rock samples by X-ray fluorescence (XRF) spectrometry with the University of Hawai'i Siemens 303AS using techniques described by Eason and Sinton (2009), consistent with the existing postglacial data presented both there and in Sinton et al. (2005). Selected XRF data are reported in Table 2, with all sample analyses reported in Supplementary Table S1 along with corresponding standards data in Supplementary Table S2.

Low-abundance trace elements were analyzed in selected postglacial and subglacial samples by inductively coupled plasma mass spectrometry (ICP-MS). Most postglacial samples were analyzed using the University of Hawai'i VG PlasmaQuad according to the methods described in Eason and Sinton (2009). Samples from subglacial and transitional units were analyzed at Washington State University on an Agilent model 4500 ICP-MS (full description of methods available at http://www.sees.wsu.edu/Geolab/note/icpms.html). Selected ICP-MS data are reported in Table 2, with all analyses reported in Supplementary Table S3.

For glass samples (glassy rinds of pillow basalts, glassy scoria, and ash samples), major and minor element concentrations were collected using the University of Hawai'i JEOL JXA-8500F five-spectrometer electron microprobe with an accelerating voltage of 15 keV, 10 nA beam current, and 20 μm beam diameter. Three to five glass chips were analyzed for each sample, with a minimum of three points (typically 4–5) measured on each glass chip. The exception to this procedure is sample IS-47, an ash layer from beneath Kjalhraun, for which multiple glass shards were analyzed from 10 separate horizons for a total of 90 point analyses (see Supplementary Table S4). Peak and background counting times were 60 s for S; 50 s for Al, K, and Mg; 40 s for Si and Ca; 30 s for Ti, Na, Fe, and P; and 20 s for Mn. Microprobe analyses were calibrated using glass standards Makaopuhi A-99 (Si, Al, Ca, Mg), Juan de Fuca VG-2 (Fe), and mineral standards sphene glass (Ti), orthoclase (K), Verma garnet (Mn), Amelia albite (Na), fluorapatite (P), and troilite (S). A ZAF matrix collection was applied to all analyses. Average glass compositions for each rock sample are reported in Supplementary Table S5.

Cosmogenic ^{3}He measurements

Only the outermost 2–3 cm of lava surfaces were sampled for helium analysis, thus minimizing corrections for depth in the lava flows. Olivine phenocrysts were separated from surface samples by crushing, magnetic separation, and handpicking. Olivine phenocrysts 0.5 to 1 mm in size (0.355–2 mm for IS-44A) were selected for purity (lack of adhering groundmass) and washed in acetone and methanol prior to measurement. The helium concentrations and isotopic compositions were measured by crushing and melting at the Woods Hole Oceanographic Institution using a 90° magnetic sector mass spectrometer. Olivine phenocrysts were first crushed in a vacuum to selectively release the magmatic helium, thought to be trapped primarily in melt and fluid inclusions. The resulting crushed olivine powder was then melted in a resistance furnace to release the helium held in the crystal matrix of the olivine, which hosts the majority of the cosmogenic ^{3}He (Kurz 1986). The quantity of magmatic ^{3}He is calculated using the measured ^{3}He/^{4}He for the helium released by crushing, while the cosmogenic ^{3}He is calculated by subtracting the inherited/magmatic ^{3}He from the total measured ^{3}He in the sample. While it has been suggested that ^{3}He production rates may vary slightly as a function of olivine composition (Lal 1991), this is unlikely to play a significant role in this study due to the relatively small compositional variation among these basaltic units (Licciardi et al. 2007). For a full description of the methodology, including assessments of data reproducibility, see Kurz (1986), Kurz et al. (1990), and Licciardi et al. (1999, 2006).

Owing to low olivine abundances in many of the units, only four new table mountain samples yielded sufficient olivine for cosmogenic helium measurement (Table 3), supplementing data for six WVZ table mountains reported in Licciardi et al. (2007). Production rates and scaling used are consistent with the local calibration reported by Licciardi et al. (2006) and are identical to those reported by Licciardi et al. (2007). All ages in this paper are reported in calendar years before present (years before 1950 A.D.) unless noted otherwise.

One sample from Þórisjökull (IS-63B) had such a small amount of gas released by crushing that the inherited ^{3}He/^{4}He value could not be determined reliably. Because the cosmogenic helium is dominant, the inherited correction is small and the resulting age calculation for this sample is

Table 2 Representative sample analyses

Sample no.	IS-1	IS-6	IS-10A	IS-31	IS-37A	IS-46B	IS-55B
Unit	Hrafnabjörg	Bitra	Hestfjall	Geitafell	Hvalfell	Kjalfell	Trölladalur
Major and trace element data by XRF							
SiO_2	48.65	49.19	48.19	48.89	48.04	48.30	48.85
TiO_2	1.81	1.25	1.75	2.13	1.68	1.45	1.28
Al_2O_3	15.57	16.81	14.84	15.30	15.36	15.53	17.20
FeO*	11.78	10.69	12.23	12.20	11.52	12.13	9.94
MnO	0.20	0.17	0.20	0.19	0.19	0.19	0.17
MgO	7.63	7.40	8.42	7.33	8.63	9.04	7.60
CaO	12.37	13.60	12.54	11.97	12.85	12.08	13.91
Na_2O	1.79	1.63	1.94	1.97	1.40	1.54	1.37
K_2O	0.20	0.07	0.13	0.32	0.18	0.11	0.05
P_2O_5	0.25	0.10	0.18	0.32	0.20	0.14	0.12
Sum	100.2	100.9	100.4	100.6	100.1	100.5	100.5
LOI	−0.52	−0.11	−0.01	−0.53	−0.12	−0.67	−0.38
Sc	41	42	37	38	42	38	40
V	313	284	304	301	341	305	283
Cr	321	216	308	289	538	403	439
Co	48	25	44	41	53	52	41
Ni	106	78	101	105	150	181	118
Cu	118	101	100	109			
Zn	97	74	86	93	93	91	65
Rb	3.8	1.3	2.4	6.5	4.2	2.6	1.5
Sr	214	184	178	237	210	158	167
Y	28	21	27	30	23	23	19
Zr	116	62	89	135	94	58	47
Nb	15.0	6.5	10.6	19.0	15.1	5.6	5.1
Trace element data by ICP-MS							
La	9.83	5.07	7.10	13.07	9.30	4.23	3.28
Ce	23.75	12.19	17.75	30.41	22.00	10.72	8.99
Pr	3.43	1.83	2.66	4.23	3.10	1.67	1.45
Nd	15.92	8.91	12.74	19.03	14.05	8.20	7.42
Sm	4.38	2.66	3.78	5.04	3.75	2.72	2.41
Eu	1.59	1.05	1.39	1.76	1.39	1.10	0.95
Gd	5.08	3.32	4.55	5.49	4.32	3.50	2.99
Tb	0.88	0.59	0.80	0.93	0.71	0.65	0.54
Dy	5.43	3.85	5.06	5.79	4.43	4.22	3.51
Ho	1.09	0.81	1.08	1.14	0.91	0.89	0.74
Er	2.96	2.25	2.92	3.08	2.45	2.41	1.98
Tm	0.42	0.32	0.40	0.43	0.35	0.35	0.28
Yb	2.56	1.94	2.50	2.58	2.11	2.20	1.73
Lu	0.39	0.30	0.40	0.40	0.33	0.35	0.27
Ba	58	32	35	87	67	31	19
Th	0.52	0.33	0.32	0.95	0.63	0.26	0.10
Hf	2.88	1.65	2.37	3.35	2.42	1.67	1.39
Ta	0.87	0.40	0.63	1.16	0.89	0.33	0.31
U	0.16	0.09	0.10	0.29	0.18	0.08	0.03
Pb	0.59	0.34	0.46	0.82	1.12	0.31	0.26
Rb	3.0	0.8	1.9	5.8	3.2	1.7	0.6
Cs	0.04	0.01	0.03	0.06	0.04	0.02	0.01
Sc	42.0	43.2	43.8	39.5	41.8	40.0	42.5

Table 2 (continued)

Sample no.	IS-61	IS-64A	IS-66	IS-69A	IS-73	IS-76A	IS-84A
Unit	Þórisjökull	Þórisjökull	Hlöðufell	Högnhöfði	Rauðafell	Stóra-Björnsfell	Skriða
Major and trace element data by XRF							
SiO_2	48.88	48.39	48.93	48.13	48.31	47.85	49.46
TiO_2	1.03	0.94	1.49	1.87	1.54	1.48	1.18
Al_2O_3	15.70	16.33	15.83	15.75	15.56	16.50	16.20
FeO*	10.24	9.85	11.50	11.78	11.16	11.18	10.61
MnO	0.17	0.17	0.18	0.19	0.18	0.18	0.17
MgO	8.85	9.75	8.21	8.32	9.33	8.82	8.49
CaO	13.86	13.27	12.51	11.92	11.97	12.26	13.35
Na_2O	1.39	1.32	1.58	1.86	2.20	1.67	1.37
K_2O	0.03	0.03	0.14	0.24	0.28	0.10	0.10
P_2O_5	0.06	0.05	0.10	0.18	0.16	0.16	0.13
Sum	100.2	100.1	100.5	100.2	100.7	100.2	101.1
LOI	−0.39	−0.39	−0.60	−0.62	−0.51	−0.49	−0.36
Sc	42	39	42	38	40	33	40
V	269	248	319	318	293	260	281
Cr	459	575	459	339	473	362	388
Co	46	50	49	52	39	48	49
Ni	130	187	162	142	181	164	130
Cu	108	101	86	118	90		
Zn	63	65	93	94	87	76	73
Rb	1.1	1.2	2.7	4.1	5.1	2.1	2.6
Sr	118	117	172	234	208	193	154
Y	18	16	23	24	21	21	21
Zr	25	23	71	96	85	65	56
Nb	2.0	1.8	7.4	13.3	13.1	7.5	5.9
Trace element data by ICP-MS							
La	1.48	1.30	5.49	9.22	8.82	5.31	4.25
Ce	4.13	3.54	13.07	20.84	19.57	12.76	10.16
Pr	0.71	0.64	2.01	3.05	2.81	1.98	1.55
Nd	4.11	3.68	9.82	14.18	12.58	9.61	7.49
Sm	1.64	1.47	3.03	3.94	3.33	2.92	2.38
Eu	0.72	0.65	1.17	1.47	1.26	1.18	0.95
Gd	2.43	2.18	3.80	4.52	3.84	3.60	3.10
Tb	0.47	0.42	0.67	0.77	0.64	0.64	0.57
Dy	3.19	2.87	4.39	4.80	4.12	4.02	3.81
Ho	0.70	0.63	0.92	0.96	0.84	0.84	0.81
Er	1.99	1.77	2.52	2.54	2.27	2.30	2.21
Tm	0.29	0.26	0.36	0.36	0.32	0.32	0.32
Yb	1.78	1.60	2.23	2.19	1.91	1.98	1.97
Lu	0.28	0.25	0.34	0.33	0.30	0.30	0.31
Ba	11	10	37	65	68	34	31
Th	0.06	0.05	0.36	0.62	0.65	0.25	0.28
Hf	0.92	0.81	1.91	2.50	2.17	1.75	1.55
Ta	0.12	0.11	0.45	0.80	0.77	0.47	0.33
U	0.02	0.02	0.10	0.19	0.20	0.08	0.09
Pb	0.18	0.15	0.44	0.64	0.62	0.35	0.41
Rb	0.5	0.4	2.3	4.0	4.6	1.7	1.8
Cs	0.01	0.01	0.03	0.05	0.06	0.02	0.02
Sc	45.6	37.8	40.0	38.6	38.5	37.4	43.1

Table 2 (continued)

Sample no.	IS-91	IS-92	IS-99	IS-107	IS-110	IS-116
Unit	Eiríksjökull	Eiríksjökull	Fanntófell	Hrútfell	Geitlandsjökull	Krákur
Major and trace element data by XRF						
SiO_2	49.34	49.98	48.99	48.47	49.19	48.16
TiO_2	1.04	1.08	1.72	1.75	1.43	1.32
Al_2O_3	17.14	18.11	14.03	16.01	16.07	15.29
FeO*	10.40	10.37	11.62	11.85	10.93	10.97
MnO	0.17	0.17	0.18	0.18	0.18	0.18
MgO	7.85	6.71	11.09	8.41	7.33	8.62
CaO	13.37	13.63	11.43	12.17	13.15	12.68
Na_2O	1.59	1.42	1.28	1.66	1.44	1.51
K_2O	0.07	0.06	0.35	0.14	0.11	0.07
P_2O_5	0.02	0.12	0.25	0.18	0.11	0.11
Sum	101.0	100.3	100.9	100.8	99.9	98.9
LOI	−0.50	−0.49	−0.35	−0.56	−0.32	−0.49
Sc	45	41	37	37	45	42
V	283	288	305	293	330	284
Cr	142	155	892	264	408	380
Co	35	43	58	36	30	36
Ni	117	86	268	156	108	166
Cu	97	88	107	110	104	
Zn	76	75	92	93	87	88
Rb	1.7	1.8	8.1	2.6	2.5	1.2
Sr	140	151	238	209	167	136
Y	20	20	22	25	23	27
Zr	41	43	106	100	74	72
Nb	3.0	3.0	18.0	12.3	8.9	6.8
Trace element data by ICP-MS						
La	2.32	2.58	12.46	8.02	5.92	4.41
Ce	6.13	6.66	27.24	19.31	14.09	11.11
Pr	1.03	1.11	3.76	2.93	2.13	1.81
Nd	5.46	5.89	16.65	13.89	10.19	9.28
Sm	2.02	2.13	4.11	3.98	3.01	3.14
Eu	0.87	0.90	1.45	1.52	1.19	1.25
Gd	2.87	2.94	4.39	4.63	3.78	4.18
Tb	0.54	0.56	0.72	0.81	0.67	0.76
Dy	3.59	3.71	4.37	4.97	4.32	5.08
Ho	0.78	0.80	0.87	1.02	0.91	1.06
Er	2.15	2.21	2.27	2.66	2.45	2.86
Tm	0.31	0.32	0.32	0.37	0.35	0.41
Yb	1.92	1.97	1.92	2.27	2.19	2.52
Lu	0.30	0.31	0.30	0.35	0.35	0.39
Ba	16	19	103	45	37	26
Th	0.13	0.16	1.06	0.34	0.30	0.13
Hf	1.22	1.29	2.68	2.50	1.89	1.97
Ta	0.17	0.17	1.07	0.72	0.50	0.38
U	0.04	0.05	0.31	0.11	0.09	0.05
Pb	0.23	0.30	0.84	0.45	0.41	0.27
Rb	0.8	1.0	7.1	2.0	1.6	0.6
Cs	0.01	0.01	0.09	0.02	0.02	0.01
Sc	40.8	40.2	37.7	39.2	42.6	41.2

Oxide abundances given in weight percent and trace elements in parts per million. Total Fe as FeO*

not particularly sensitive to that parameter. Using the highest measured magmatic (crushing) $^{3}He/^{4}He$ value obtained for the age calculation would yield an exposure age lower by 5 %. We note that this sample is also extremely depleted in incompatible trace elements (see section on "Geochemical composition"), which is consistent with the exceptionally low magmatic ^{3}He measured.

Results

Tuya geology

Selected geological observations are summarized in Table 1, including passage zone heights, estimated eruptive volumes, and extent of modification of lava surfaces. More detailed descriptions of the lava surface and other related geologic observations can be found in Table S6 in the Supplementary Material. Although some units have a single, well-defined passage zone contact (e.g., Hrútfell, Eiríksjökull, Þórisjökull), the transition between subaqueous and subaerial eruptive styles is more complex for many units. Some tuyas have multiple passage zones, locally producing a bench-like morphology (e.g., Hlöðufell, Fig. 2b) (Skilling 2009). The local presence of multiple passage zones could reflect fluctuating lake levels during a single continuous eruption or mark multiple eruptive episodes. Lava delta foreset breccias are common immediately below (or interbedded with) the lowest subaerial lava flows and were likely deposited when subaerial capping lava flowed into the ice-confined lake. Several tuyas have scoria cones and sheets composed of glassy scoria just above the passage zone or close to the summit region (e.g., Hestfjall, Kjalfell, Hlöðufell, Skriða; Fig. 2c, d). In addition to table mountains with subaerial capping lava, we also sampled Kálfstindar and Litla-Björnsfell, which lack subaerial lava flows.

Units we refer to as "transitional" have thin subaqueous sections (most <200 m thick) that extend less than halfway around the perimeter of the unit. The relatively small proportion of subaqueous lithologies indicates more limited water interaction during their eruption and suggests that the ice sheet present during their eruption, if any, was too thin or not extensive enough to confine glacial meltwater for much of the eruption's duration.

Some tuyas have mappable subunits with mineralogical differences visible in the field. Most of Eiríksjökull surmounts a less vesicular lower subunit with less plagioclase (~10 vs.

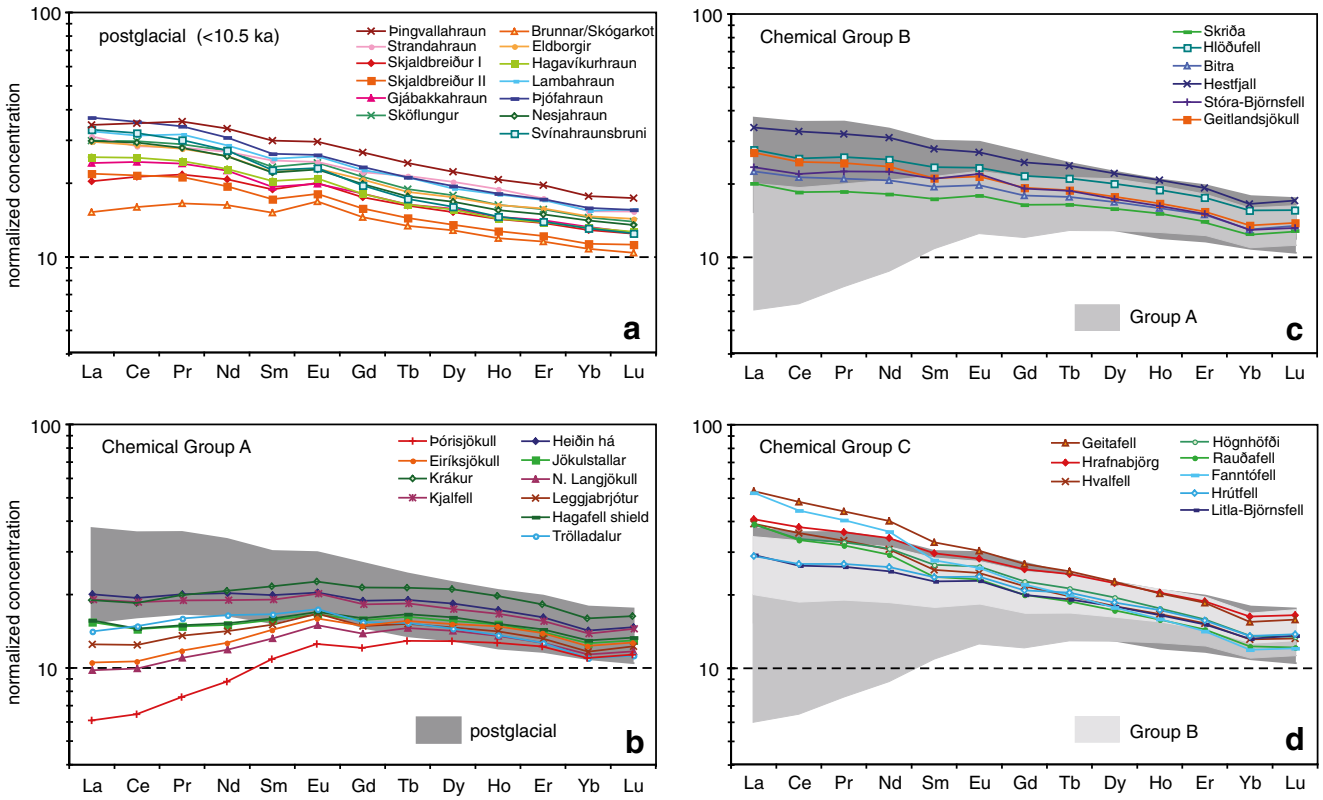

Fig. 3 Rare earth element (REE) concentrations normalized to primitive mantle of McDonough and Sun (1995). **a** Postglacial units of the WVZ, **b** Chemical Group A (including both subglacial and transitional units), **c** Chemical Group B, and **d** Chemical Group C. Data are unit averages (~2–3 samples per unit). Depletions in light rare earth elements characterize Group A subglacial and transitional units, in contrast to other subglacial and later postglacial units

Table 3 New helium isotope data for WVZ units

Sample	Unit	Olivine (g)	Altitude (km)	Latitude	Longitude	$^3He/^4He$ (R/R_a, crush)	$^3He/^4He$ (R/R_a, melt)	^4He (10^{-10} cm^3 g^{-1})	^3He_c (10^5 at g^{-1})	Scaling factor	Age (ka, ±1σ)
IS-44A	Kjalfell	0.1244	0.981	64.7749	−19.5329	11.2±0.6	220±4	4.2±0.2	32.2±1.9	2.518	9.9±0.6
IS-51B	Heiðin há	0.2904	0.597	63.96345	−21.6284	12.2±0.6	213±4	2.9±0.1	21.8±0.9	1.801	9.3±0.4
IS-63B	Þórisjökull	0.2819	1.027	64.5349	−20.8079	1.9±1.0	255±4	4.2±0.1	29.4±1.2	2.617	11.6±0.6
IS-76B	Stóra-Björnsfell	0.2597	0.972	64.4917	−20.7182	8.8±0.5	70.0±1.3	10.0±0.1	23.0±0.6	2.499	7.1±0.2

Helium measurement uncertainties based on a 0.5 % uncertainty on the ^{4}He peak and an error of 2×10^{12} cm^3 STP (about 3 %) on the blank. $^3He/^4He$ ratios are reported relative to the atmospheric value (R/R_a where $R_a=1.386\times10^{-6}$). For all samples, crushing and melting were performed on the same mineral separately. Scaling factors are the ratio of production at sample location to production at sea level at high latitudes, following Table 2 in Lal (1991). Uncertainties of individual exposure age determinations include propagated 1σ analytical uncertainties only

20 % or more for most samples, and mostly clustered in small glomerocrysts) and more abundant olivine (>5 vs. 1–3 %). However, these two subunits are not chemically distinguishable (Supplementary Material Fig. S1). The presence of subaerial flows at the same elevation as the subaqueous hyaloclastite of the lower subunit indicates that water levels dropped significantly during the eruption; the passage zone elevation is 300–400 m lower on average on the eastern side of the edifice than on the western side. Similarly, Krákur consists of a lower sequence of pillows and hyaloclastite breccia containing ~15 % olivine, overlain by nearly aphyric pillow lavas and subaerial flows that comprise the rest of the tuya. Along with less olivine, samples from the upper subunit have lower MgO contents than the lower sequence, but the two lithologies have identical trace element ratios (e.g., K/Ti, Zr/Y, Nb/Y), and appear to be related by fractionation (Fig. S1). Hrútfell is built on a low-lying, pillow-dominated pedestal (total extent unknown) that contains only 1–3 % olivine phenocrysts, in contrast to porphyritic (~15 % plagioclase and 5 % olivine) lavas that make up the main body of Hrútfell. In this case, chemical data (Fig. S1) indicate that the two units of Hrútfell are unlikely to be comagmatic (see Discussion section Monogeneity and eruptive style).

Although most WVZ tuyas are isolated edifices, hyaloclastite breccia that we interpret to be part of Þórisjökull laps onto the flanks of Geitlandsjökull (Fig. 2f), indicating that Þórisjökull is younger than Geitlandsjökull; Þórisjökull hyaloclastites also partially bury a fault scarp near its southwestern end (Supplementary Material), providing further evidence for a relatively young age for this tuya.

Geochemical composition

WVZ tuya samples span a considerable range in extent of differentiation and incompatible element enrichment. We have subdivided them into three main chemical groups using chondrite-normalized (denoted by superscript N) lanthanide rare earth element (REE) ratios (Fig. 3)—Group A: incompatible element-depleted units, $La/Sm^N \leq 1.0$; Group B: $La/Sm^N > 1.0$ and $La/Lu^N \leq 2.0$; and Group C: incompatible element-enriched units with inclined REE patterns, $La/Lu^N > 2.0$. New REE data from WVZ postglacial lavas show that they have REE patterns that are most similar to our Chemical Group B (Fig. 3).

Chemical Group A comprises all of the transitional units in the WVZ except Bitra and Hestfjall, as well as Þórisjökull, Eiríksjökull, Krákur, and Kjalfell table mountains. In addition to their flat to light REE-depleted patterns (Fig. 3b), these samples have correspondingly low ratios of other highly incompatible to moderately incompatible elements. They also define extremes in major element compositions, extending to lower TiO_2, K_2O, and P_2O_5 contents at a given MgO

than other WVZ subglacial units (Fig. 4), and tend toward higher CaO and SiO_2 and lower FeO*, although there is more overlap in these oxides. Þórisjökull, Eiríksjökull, and N. Langjökull have the most extreme trace element depletions of any subglacial units in this study.

Chemical Group B includes southern transitional units Bitra and Hestfjall and tuyas Skriða, Hlöðufell, Geitlandsjökull, and Stóra-Björnsfell. This group is compositionally intermediate to groups A and C, with REE patterns that are the most similar to postglacial lavas (Fig. 3) and fairly moderate major element oxide concentrations overall (Fig. 4).

Chemical Group C units, which have inclined REE patterns (Fig. 3a), tend to have high TiO_2, K_2O, P_2O_5, and other elements that behave incompatibly during mantle melting (Fig. 4). Groups B and C both tend to have lower CaO and slightly higher FeO* than most Group A lavas (Fig. 4). This group includes units Fanntófell, Geitafell, Högnhöfði, Hrafnabjörg, Hrútfell, Hvalfell, Rauðafell, and Litla-Björnsfell.

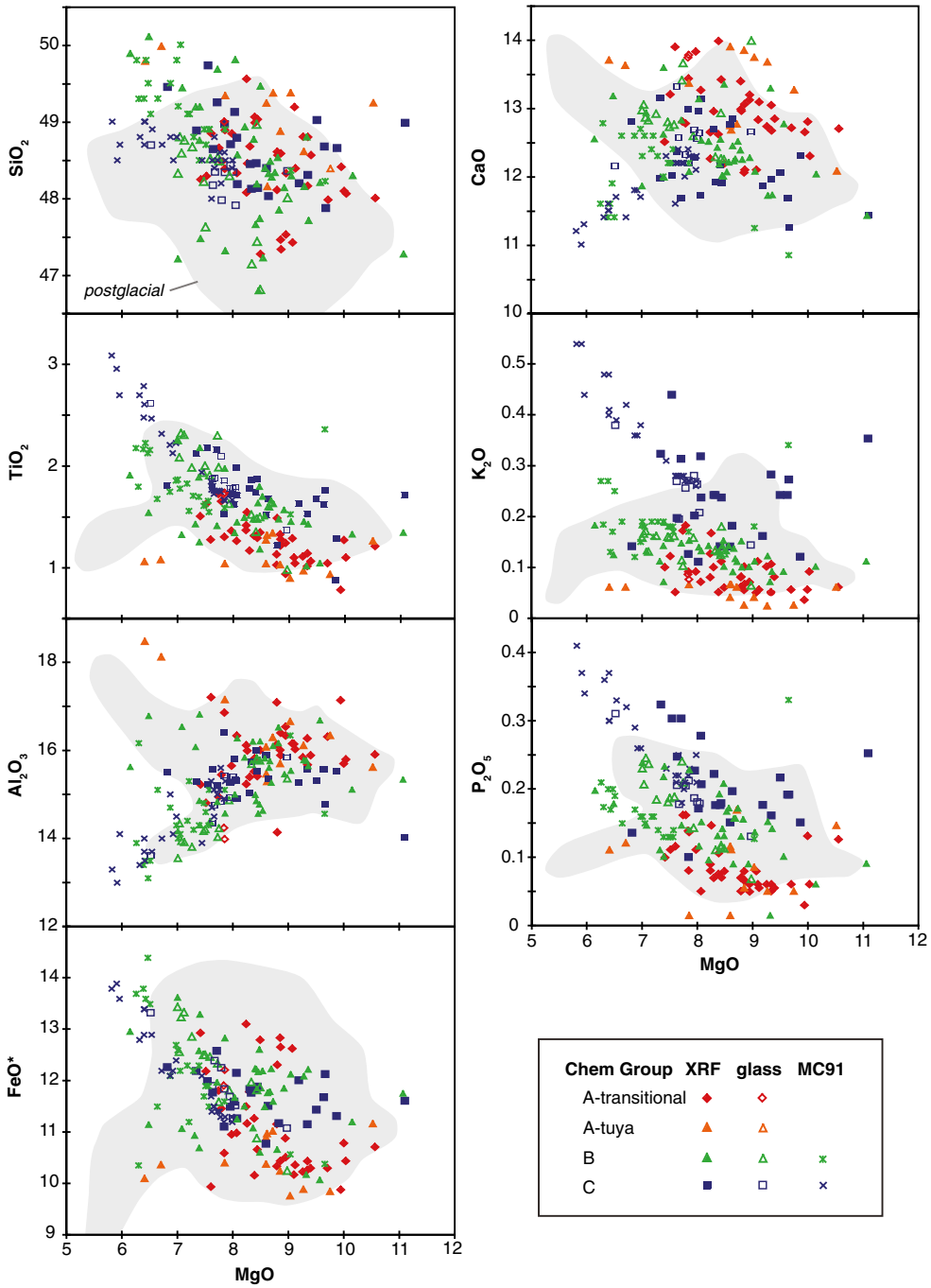

Fig. 4 Major element chemical variations of transitional units and table mountains in the WVZ, color-coded by chemical group (see Table 1 and text for group definitions). *Filled symbols* denote whole rock data, *open symbols* denote glass data. Also plotted are glass data for selected units from Moore and Calk (1991) (MC91). *Gray fields* encompass glass and whole rock data for WVZ postglacial lavas (excluding picrites) from Sinton et al. (2005) and Eason and Sinton (2009)

All samples, regardless of chemical group, have positive Eu anomalies that are most evident in the least differentiated samples with high MgO and low Yb concentrations. These same samples also have positive Sr anomalies, which decrease and eventually become negative with increasing extents of differentiation. The decrease in Eu and Sr anomalies with increasing Yb is consistent with plagioclase fractionation, which preferentially removes these elements from the melt. The positive Eu and Sr anomalies in the less evolved magmas are unlikely to be the result of plagioclase accumulation, despite plagioclase abundance locally up to ~20 % phenocrysts, because the magnitude of the positive Eu anomalies does not correlate with modal mineralogy. We therefore favor the alternative explanation that melting of recycled, plagioclase-rich lithologies in the upwelling source beneath the WVZ may produce positive Eu and Sr anomalies in the primary magmas (e.g., Chauvel and Hémond 2000; Sobolev et al. 2000).

Many individual tuyas show internal chemical variation, with lavas becoming increasingly differentiated up section. In each of the ten edifices for which we have both subglacial (pillow lavas and pillow clasts in hyaloclastic pillow breccias) and subaerial whole rock data, the subaerial lavas consistently have lower MgO than their subglacial counterparts (Supplementary Fig. S2). Decreasing MgO with stratigraphic height also was observed in glass data on a limited number of features by Moore and Calk (1991), and several postglacial lava shields show decreasing MgO toward their summits (Sinton et al. 2005; Eason and Sinton 2009). Declining MgO is consistent with increasing differentiation, which likely accompanies declining magma supply during later stages of subglacial lava shield evolution.

Subaerial lava surfaces

We observe a wide range of lava surface preservation among the different edifices of the WVZ, varying from pristine surfaces equivalent to those on early postglacial lavas, to highly modified, scoured and locally eroded surfaces. Although individual edifices can show a range of surface preservation across their summits, this range is limited for any individual edifice. We distinguish four distinct categories of lava surface quality based on how common or pervasive surficial modification is across all observed areas for a given edifice.

Surface Category I units exhibit little to no surface modification beyond the typical amounts of weathering observed on older postglacial units. Ropes, crustal rinds, and other delicate surface structures are common on lava surfaces in this group, which includes all of the transitional units as well as the remarkably well-preserved capping lava of Þórisjökull (Fig. 2e).

Units in Surface Category II exhibit mild to moderate amounts of surface modification; the outermost few centimeters of surfaces commonly have been removed, but some ropy pāhoehoe structures, small channels or inflationary lobes, and similar primary flow features can still be recognized locally. Tuyas in this category include Bitra, Eiríksjökull, Hestfjall, Hlöðufell, Kjalfell, Krákur, and Skriða (Table 1).

Surfaces for Categories III and IV are more extensively modified. Category III lavas are generally shattered and blocky, with moderate to extensive removal of the outermost parts, such that little to no original lava surface remains. In some cases, individual flow units are still discernible even though the surfaces are no longer continuous. Some units show signs of possible glacial scouring, but the evidence is ambiguous or inconsistent in the areas we traversed. Tuyas in this group include Geitafell, Geitlandsjökull, Hrafnabjörg, and Hvalfell. Units in Category IV (Fanntófell, Högnhöfði, Rauðafell, Hrútfell, Stóra-Björnsfell) show extensive surface removal with explicit signs of glacial erosion, including glacial striae, scouring and/or polish and, in some cases, the beginnings of valley erosion.

Modification of lava surfaces on high-elevation table mountains receiving frequent snowfall, profound diurnal and seasonal temperature variations and possibly prior cover by glacial ice can be expected to reflect both the time since formation and local variations in snow pack, ice thickness, temperature, and underlying slopes. The most profound effects accrue when thick ice moves downslope, abrading the underlying lava surface. The absence of glacial evidence on a particular unit does not necessarily preclude the possibility of it having been covered for some time after it formed, as long as the snow and ice was relatively stagnant and generated little erosion. Ice toward the stable interior of an ice sheet might have low velocity compared with the more active outer margins, or, if conditions were cold enough, the base of the ice could have been frozen to the underlying bedrock, as occurs in some polar glaciers (e.g., Goodfellow 2007). Thin glaciers are unlikely to flow, and it is therefore possible that some tuyas could have experienced extended periods of ice burial without exhibiting much surface damage. Even in the absence of glacial ice, harsh climates with frequent freeze-thaw cycles can enhance weathering of the outer crust, or cause extensive fracturing and shattering of the lava surface, creating blocky, jumbled surfaces out of originally smooth, continuous flow units.

These local effects arising from variations in latitude, elevation, and localized climate can overprint the effects associated with the general changes in temperature and amount of ice present during the transition out of the last glacial period, which makes a direct correlation between the extent of surficial damage and age highly tenuous. Nevertheless, the presence of unmodified,

pristine lava surfaces is more likely to characterize relatively young lava flows, whereas the total lack of original flow surfaces, especially where there is evidence of glacial scouring and polish, clearly indicates post-eruptive covering by glacial ice of significant thickness.

^{3}He exposure ages

New cosmogenic ^{3}He concentrations and calculated exposure ages for each unit are presented in Table 3. We do not correct for geomagnetic modulation of ^{3}He production rates because cosmogenic nuclide production at high latitudes is thought to be insensitive to changes in the magnetic field (Gosse and Phillips 2001; Pigati and Lifton 2004; Licciardi et al. 2006).

Licciardi et al. (2006, 2007) discussed uncertainties associated with cosmogenic exposure dating of Icelandic table mountains. Glaciation and other forms of burial temporarily block cosmic rays, leading to exposure ages that are younger than the actual age of formation. Surface erosion and snow cover lead to additional offsets from eruption age. The cosmic ray neutron-induced spallation reactions that produce cosmogenic ^{3}He decrease exponentially with depth in the rock, and while some correction can be made by adjusting the effective production rates, this requires knowing erosion rates from some other method.

Only if a lava flow has been continuously exposed to cosmic rays since eruption and not undergone significant erosion or cover will an exposure age equal the eruption age. In all cases, the major sources of uncertainty inherent in this method result in ages that are anomalously low (too young). For example, the published exposure age determined for Hlöðufell of 8.2 ka (Licciardi et al. 2007), a time when this part of the WVZ was almost certainly completely ice free, is too low to be the age of formation and therefore probably reflects either surface removal or a significant period of burial. Subsequent sampling from well-preserved, high-standing tumuli surfaces on this tuya summit yielded a revised age of 10.7 ka (Licciardi, personal communication). Similarly, the sample from Stóra-Björnsfell, which shows evidence for glacial scouring elsewhere on the summit, yields an erroneously young age (7.1 ka). Thus, owing to the effects of long-term burial on cosmogenic ^{3}He production, we regard all cosmogenic exposure ages as minima for the eruption age. We estimate that exposure ages may be less than the actual eruption age by as much as several thousand years in some cases, particularly for the highest peaks around Langjökull (e.g., Þórisjökull, Eiríksjökull, Geitlandsjökull, Hrútfell, and perhaps Krákur and Hlöðufell), where recent modeling suggests that this region may have hosted a substantial permanent snow cover or passive glacier for most of the past 2000 years (Flowers et al. 2008). Exposure ages should be closest to actual eruption ages for postglacial units and the least modified tuya units, with declining confidence for older and/or more modified units.

Revisions to postglacial eruptive history

Postglacial geochemical data and an eruptive history for the postglacial WVZ were presented in Sinton et al. (2005). Here we revise the age estimates of two of those units and describe two additional eruptive units in the southern WVZ not recognized by Sinton et al. (2005).

Sinton et al. (2005) noted that Kjalhraun is immediately underlain by a distinctive black ash up to 15 cm thick and speculated that this ash might represent an early explosive phase to the Kjalhraun eruption. We have since discovered a better-preserved ash section more than 1 m thick beneath Kjalhraun to the east of Kjalfell. New chemical data indicate that the section is mostly chemically uniform (Supplementary Table S3), except for one anomalous horizon high in the section (IS-47B) that has higher Ti and K, similar to known compositions from Katla. All other analyses match that of the basaltic Saksunar ash, which likely erupted from Grímsvötn in the Eastern Volcanic Zone 10,347±45 ice core years B.P. (Svensson et al. 2008 and references therein). Because there is no intervening layer of soil, we estimate the age of Kjalhraun to be ~10,000 years B.P., more than 2000 years older than the ~7800 years B.P. estimate of Sinton et al. (2005) based on the correlation of a silicic ash layer ~22 cm above the Kjalhraun lava with Hekla 5.

^{3}He exposure dating provides a new minimum age estimate for Heiðin há, a transitional unit in the southern WVZ, of ~9300 years B.P. This area is thought to have been completely ice free by then (see earlier section on "Glacial chronology"), and the limited subaqueous eruptive portion of this unit could be the result of interaction with liquid water not associated with glacial ice. We also distinguish a new unit, Strandahraun, as being chemically distinct from Heiðin há (see Supplementary Table S3) consistent with the mapping of Jónsson (1978) and Sæmundsson et al. (2010). In addition, geological relations (Sæmundsson et al. 2010) indicate that these units are all likely younger than Hlíðarhraun, the small d18 picrite of Jónsson (1978). Thus, there are at least four postglacial compound lava units in this area (Hlíðarhraun, Strandahraun, Hafnarhraun, and Selvogsheiði) that are all older than Heiðin há. These earlier, only partially exposed, units lack evidence for ice or water interaction.

In addition, we have modified the map area of Hallmundarhraun to show the presence an older lava, called Borgarhraun by Jakobsson (2013), which he estimates to be 1800-4500 years old. We also consider NE Langjökull and Jökulkrókur to be part of the same eruptive unit, as previously suggested by Sinton et al. (2005). Limited samples are geochemically indistinguishable, and although poorly exposed

beneath glacial deposits and the edge of the current ice cap, topographical relations suggest that they could be distal flows from a single, larger lava shield that mainly lies beneath Langjökull.

Discussion

Monogeneity and eruptive style

Some of the tuyas in our study exhibit mappable subunits with mineralogical differences visible in the field, raising the question of whether any of these compound features might actually represent more than one unrelated eruption. In the discussion below, an "eruption" may contain separate eruptive phases, go through periods of quiescence, and span months to decades, but its products consist of material from a single, chemically coherent magma source.

Eiríksjökull and Krákur can each be divided into lower and upper subunits with differences in mineralogy and passage zone (see Supplementary Material). Both horizons within Eiríksjökull are plagioclase-phyric with similar, distinctive chemical characteristics, including incompatible element depletions that are extreme for the WVZ (Supplementary Material Fig. S1). We therefore interpret the two parts of Eiríksjökull to be comagmatic and to represent different phases of a single eruption. A lower sequence at Krákur consists of olivine-phyric (~15 %) pillows and hyaloclastite breccia, overlain by nearly aphyric pillow lavas and subaerial flows that comprise the rest of the tuya. Substantial scatter in the whole rock major element data partly reflects variable phenocryst contents and a liquid line of descent is not well defined (Fig. S1). Despite the striking difference in mineral mode, the two lava types have nearly identical incompatible trace element ratios, consistent with the interpretation that these units could have erupted from the same magma reservoir (Fig. S1).

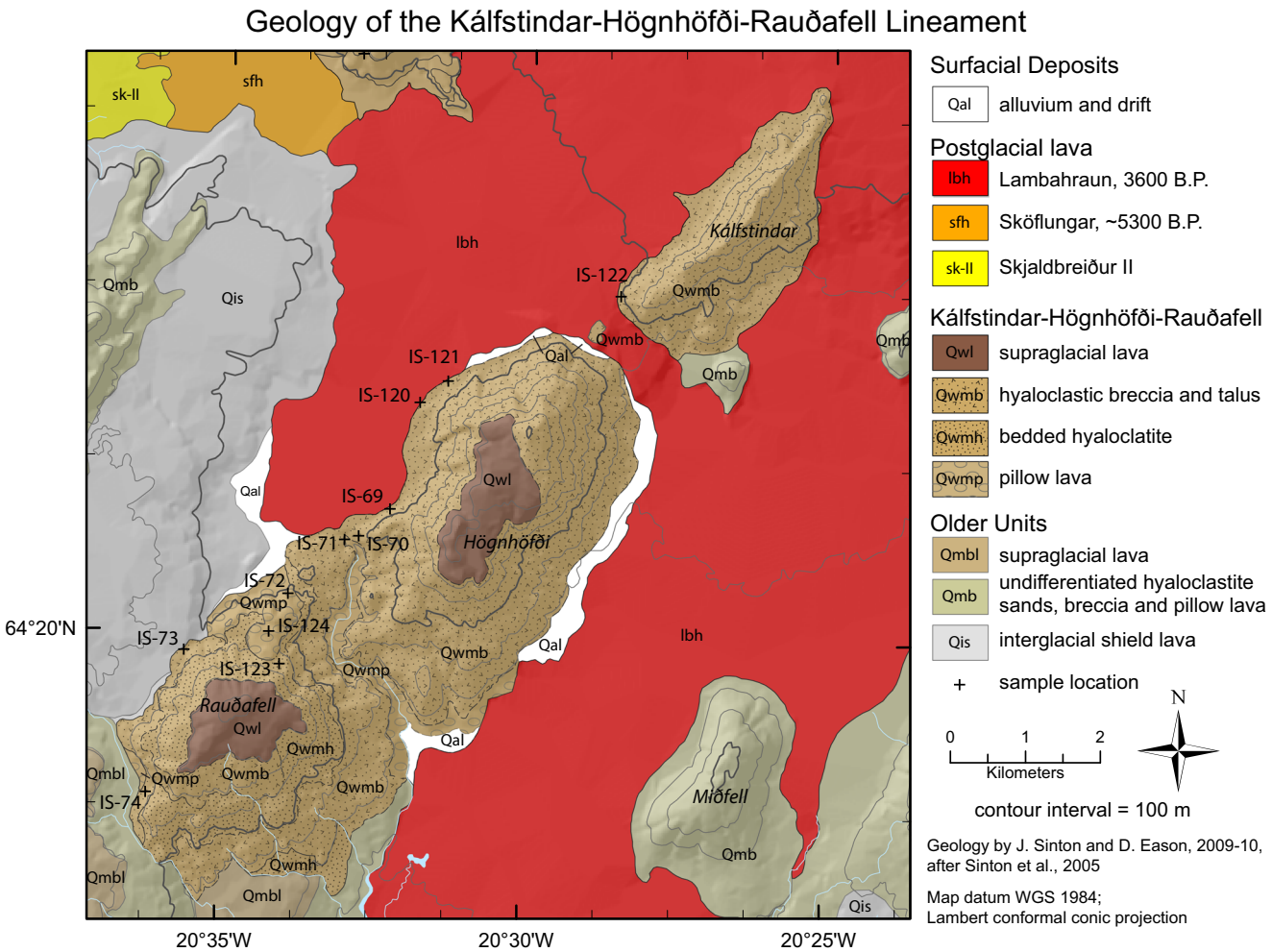

Fig. 5 Geologic map of the Kálfstindar-Högnhöfði-Rauðafell lineament. *Crosses* (+) denote sample locations. The three edifices are colinear, striking N45° E. Chemical and lithological data are consistent with all three features being produced during a single eruption (see text for discussion)

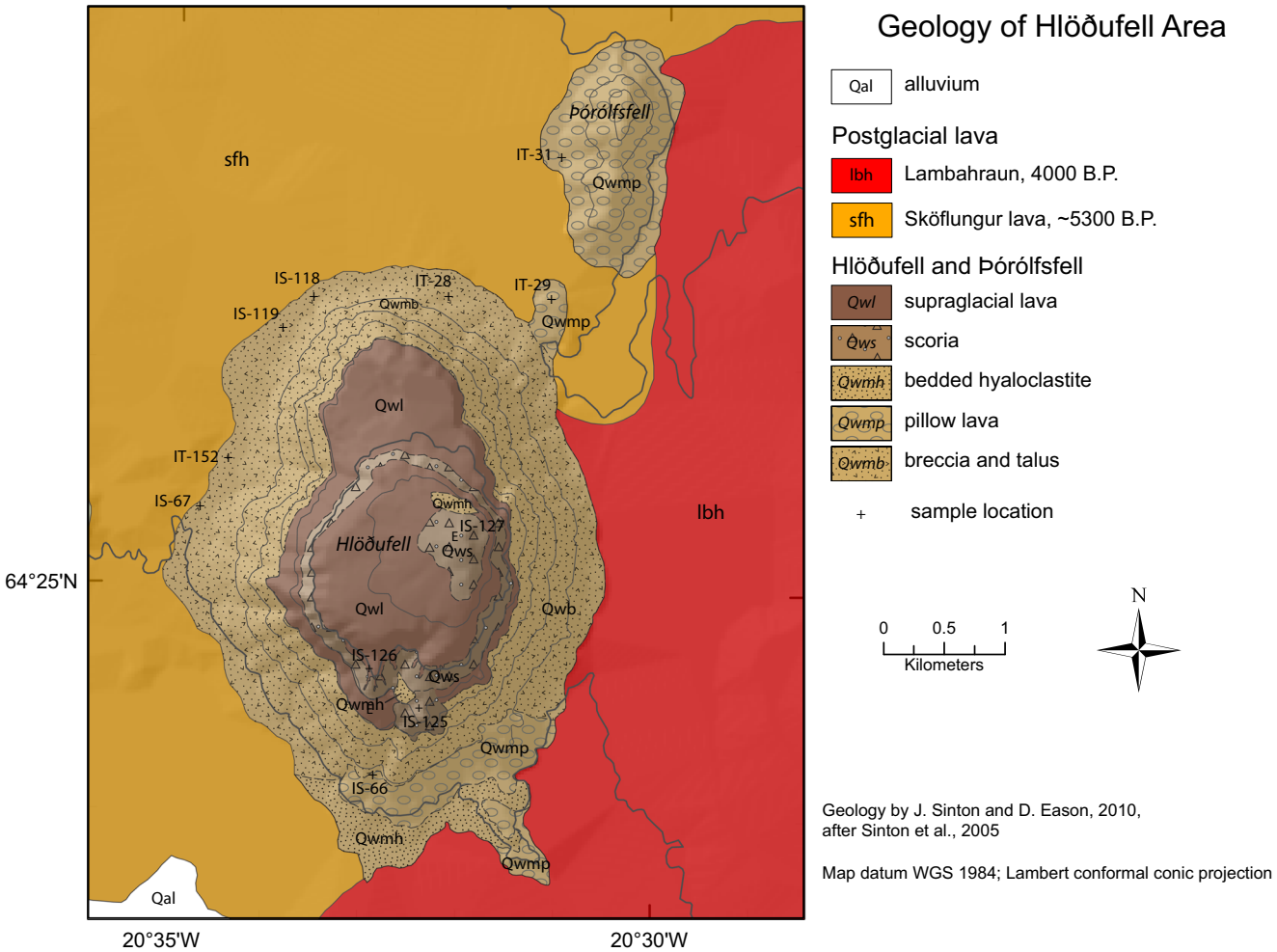

Fig. 6 Geologic map of the Hlöðufell area. *Crosses* (+) denote sample locations. Note two horizons of subaerial lava, separated by a sheet of scoria on Hlöðufell, indicating a change in eruptive style. Hlöðufell tuya is built on a sequence of hyaloclastites and pillow lavas that extend northward to include Þórolfsfell, which we consider to represent early eruptive products of the same eruption that formed Hlöðufell

In contrast to the chemical and lithological variations at Eiríksjökull and Krákur, Hrútfell appears to be built on a low-lying pedestal of pillow-dominated subglacial material that is chemically unrelated to the main edifice. In this case, significant changes in mineralogy and topography correspond with trace element compositions that cannot be related by magmatic differentiation (Fig. S1); we suggest that the lower pedestal of Hrútfell formed from an earlier eruption and is unrelated to the overlying tuya. Our volume calculation for Hrútfell excludes this lower pedestal.

Two adjacent table mountains Rauðafell and Högnhöfði were interpreted by Licciardi et al. (2007) as relatively unmodified features differing in age by ~2000 years. However, Moore and Calk (1991) described them as "glaciated" and Jones (1969) noted that both are built on a continuous sequence of olivine-rich pillow lava. Not only is there a single basal pillow layer, but overlying the pillows, both features comprise similar, coarse-grained hyaloclastite breccias, with poorly developed bedding that is generally consistent across both units. We recognize no discernible geological boundaries between them. Both edifices are surmounted by massive, plagioclase-phyric subaerial lava. Our observations confirm the eroded nature of Rauðafell and Högnhöfði, which are separated by an erosional valley or wash. Breccias similar to those on Rauðafell and Högnhöfði also comprise Kálfstindar, a tindar northeast of Högnhöfði separated by a narrow finger of postglacial lava (Fig. 5). Rauðafell, Högnhöfði, and Kálfstindar lie along a N45° E trend that is subparallel to regional volcanic lineaments in this part of the WVZ (Sinton et al. 2005). Whole rock geochemical data for Kálfstindar and Rauðafell are similar despite some scatter, while Högnhöfði data are offset to lower MgO and inconsistently offset in other major elements (Fig. S1). The scatter of the whole rock data likely reflects the varying amounts of crystal accumulation that characterize these units. Glass data for Rauðafell, Högnhöfði, the basal pillow unit that underlies them, and

Kálfstindar form geochemically coherent trends (Fig. S1), and the glass and whole rock data from all three features define major and trace element trends that are consistent with crystal fractionation from a single parental magma. Taken together, coherent chemical trends, generally similar extents of erosion, identical internal lithological constitution, and collinearity parallel to overall trends in the WVZ suggest that these three features represent the eroded remnants from a single eruption along a ~10-km-long fissure trending N45° E. If so, the 2000-year difference in cosmogenic exposure ages (Licciardi et al. 2007; Table 1) must reflect differences in post-formation erosion, depth within the lava surface, and/or burial by snow and ice.

Similarly, we propose that Hlöðufell and Þórólfsfell, a small neighboring pillow lava mound just to the northeast, are part of the same eruptive unit. Pillows on the south side of Hlöðufell are lithologically similar to those at Þórólfsfell, and the inferred vent locations from these two subglacial features (Skilling 2009) lie on the same NE-SW trend that dominates this section of the WVZ (Fig. 6). The two available geochemical analyses from Þórólfsfell lie well within the compositional range of Hlöðufell for all elements analyzed (Fig. S1), supporting the interpretation that these two units are comagmatic.

The interpretation that separate but collinear subglacial edifices are coeruptive has implications for the styles of volcanic activity during subglacial eruptions. We propose that the Hlöðufell-Þórólfsfell and Rauðafell-Höfnhöfði-Kálfstindar sequences likely began as eruptions from fissures ~5 and 10 km long, respectively, before focusing to localized eruptive centers that built tuyas. Localization during fissure eruptions is common in recent eruptions in Iceland (Thorarinson et al. 1973; Wadge 1981; Harris et al. 2001) and has been proposed for some postglacial lava shields (e.g., Rossi 1996; Eason and Sinton 2009). Furthermore, the recognition of multiple eruptive phases within some individual tuyas indicates that table mountain and lava shield formation can be episodic, as is well documented for some postglacial, fissure-fed eruptions (e.g., Sæmundsson 1991).

With the exceptions noted above, the new geological observations and chemical data are generally consistent with the interpretation that most tuyas in the WVZ are monogenetic, representing the products of single eruptions. However, the sampling density of individual edifices in this study is far less than that of, for example, Maclennan et al. (2003) or Eason and Sinton (2009) and is insufficient to fully evaluate this relation. Additionally, previous studies of table mountains and large lava shields have noted that MgO contents tend to decrease with increasing height in the edifice (~ eruption time), in some cases correlated with changes in trace element ratios (e.g., Moore and Calk 1991; Eason and Sinton 2009), which creates added complications for assessing monogeneity from small sample sets.

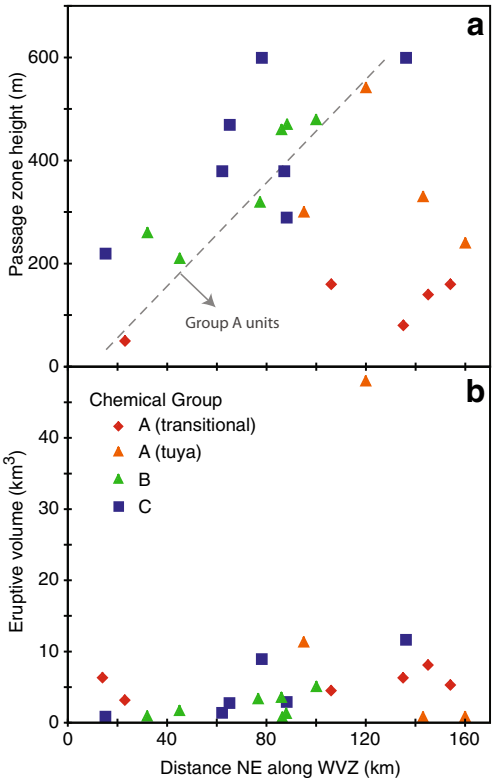

Fig. 7 Plot of **a** maximum passage zone height (transition between subaqueous and subaerial eruptive styles) and **b** eruptive volume for each unit with approximate distance NE along the WVZ (0 at the south coast). *Symbols* denote chemical group. Note that units in Chemical Group A tend to have lower passage zone heights than other units at a given latitude and that those in Chemical Groups B and C range to larger volumes with greater distance from the coast

The total volumes of Eiríksjökull and Þórisjökull make them among the largest single eruptive units yet recognized in Iceland, with important implications for their underlying magmatic processes. The combination of large volumes (up to ~48 km^3, Table 1) and lava morphologies that indicate low average effusion rates require that these can be very long-lived features, unlikely to have erupted from magma chambers with sizes as great as their erupted volumes. Rather, we favor the interpretation that these features formed by eruptions that were sustained by continuing magma recharge from the mantle, as proposed for Icelandic lava shields (Sinton et al. 2005). Such a process would be expected to contribute to geochemical heterogeneity within the edifices.

Passage zone height and eruption conditions

Tuya passage zone heights have been used to place minimum constraints on ice sheet thickness, but considerable uncertainties and variability make a direct conversion to total ice thickness difficult. Intraglacial lake surface elevation is partially controlled by drainage outlets, either limited by the lowest spillway or, in cases where the water is able to float the ice

and drain out the base, could represent the critical volume of water capable of being contained by the surrounding glacial walls (e.g., Smellie 2000; Gudmundsson et al. 2004). Smellie (2000) suggested that lake levels might be 10–15 % lower than the elevation of their host glacier, while later observations during the 1996 subglacial eruption at Gjálp showed that the lake levels were 20–25 % lower than the total ice elevation (Jakobsson and Gudmundsson 2008).

Although we are unable to determine precisely the total ice sheet thickness from passage zone heights, we note that tuyas with the highest passage zones are all in the northern half of the WVZ, consistent with the original ice sheet being thickest at high elevations near the center of Iceland and thinner near the coast (Fig. 7a) (e.g., Walker 1965; Hubbard et al. 2006). Subaqueous facies constitute only a small proportion of the total volume of the transitional units, consistent with them having formed after ice had significantly retreated from the region. Although passage zone contacts on most units are roughly horizontal, three units in the southern WVZ (Geitafell, Bitra, Hestfjall, Fig. 2c) have relatively low maximum passage zone heights that dip up to ~5° to the south, away from the interior, and Bitra, Trölladalur, and Heiðin há contain subaqueous facies almost exclusively on their northern perimeters. If the dipping passage zones are a primary feature, these units may have erupted through a relatively thin ice sheet incapable of keeping an intraglacial lake confined for the duration of the eruption. More likely, the southward dips of the passage zones could reflect differential rebound with increasing degree of uplift toward the center of Iceland. Further north in the WVZ, Eiríksjökull's passage zone dips ~2° to the west, away from the likely center of glacial loading, also consistent with differential rebound. Hyaloclastite sequences for some eruptive units south of Thingvallavatn (Bitra, Hestfjall, Geitafell) indicate that at least ~200–300 m of water was present when they were erupted.

Deglaciation and volcanism

Decompression melting is the dominant mechanism for melt generation beneath spreading centers and oceanic islands wherein hot, upwelling mantle material crosses its solidus and begins to melt. In a steady-state spreading system with uniform plate separation, this process should result in nearly constant melt production rates through time. However, rapid melting of a large ice sheet during deglaciation in Iceland temporarily increased decompression rates in the underlying mantle, resulting in increased melt production. Numerical modeling by Jull and McKenzie (1996), which assumes an axisymmetric ice load with a radius of 180 km and a maximum central thickness of 2 km that melts steadily over a period of ~1000 years, predicts average melting rates during glacial unloading to be ~30 times greater than for steady-state decompression melting controlled by plate spreading. While actual unloading was more prolonged and likely occurred in stages, this modeling demonstrates the viability of glacial unloading to produce the observed increases in early postglacial volcanic production in the neovolcanic zones of Iceland. The recent studies of Pagli and Sigmundsson (2008) and Schmidt et al. (2013) highlight the potential effects of glacial melting even in recent time, with estimates of up to 0.23 km^3/year of new magma being produced beneath Iceland in association with isostatic uplift rates up to 25 mm/year during the last century.

Geochemical variations

Mantle decompression associated with deglaciation causes increased melting rates in the shallow parts of the melting region, where the residual mantle has been depleted in incompatible elements by deeper melting. This effect has consequences for resulting magma compositions, with the amount of incompatible element depletion depending on both the rate of additional decompression and the profile of melt fraction versus depth (Jull and McKenzie 1996; Slater et al. 1998; Maclennan et al. 2002). Sinton et al. (2005) noted substantial depletions in incompatible elements in transitional and early postglacial units in the WVZ. Samples from tuyas in Chemical Group A also share this geochemical signature. Decompression associated with deglaciation provides a mechanism for generating the extreme trace element depletions and low-pressure melting signatures found in these units.

WVZ subglacial and transitional units in Chemical Groups B and C have trace element compositions within the expected range for normal melting models of a reasonable mantle composition for Iceland (Fig. 8). In contrast, most units from Group A, along with some early postglacial eruptive units and the picrite units Ásar and Búrfell (whose ages are not well constrained but also thought to be early postglacial), have trace element compositions that are more depleted than can be produced by simple partial melting (i.e., aggregated fractional melts produced by decompression melting during passive upwelling due to plate spreading) of a reasonable Icelandic mantle.

Coincident with the strong trace element depletions, Group A subglacial units and some early postglacial units have high SiO_2 and CaO and low FeO contents (Figs. 4 and 8b), consistent with enhanced melting in the uppermost mantle, as is predicted for deglaciation-induced perturbations to mantle melting. Low-pressure peridotite melting experiments generate melts with higher SiO_2 and CaO (at moderate melting extents before clinopyroxene is depleted from the residue) and lower FeO than melting at higher pressures (Jaques and Green 1979; Hirose and Kushiro 1993; Kushiro 1996; Hirschmann et al. 1999; Wasylenki et al. 2003). Early postglacial lavas in the NVZ also have lower FeO and higher CaO contents than older subglacial units erupted prior to

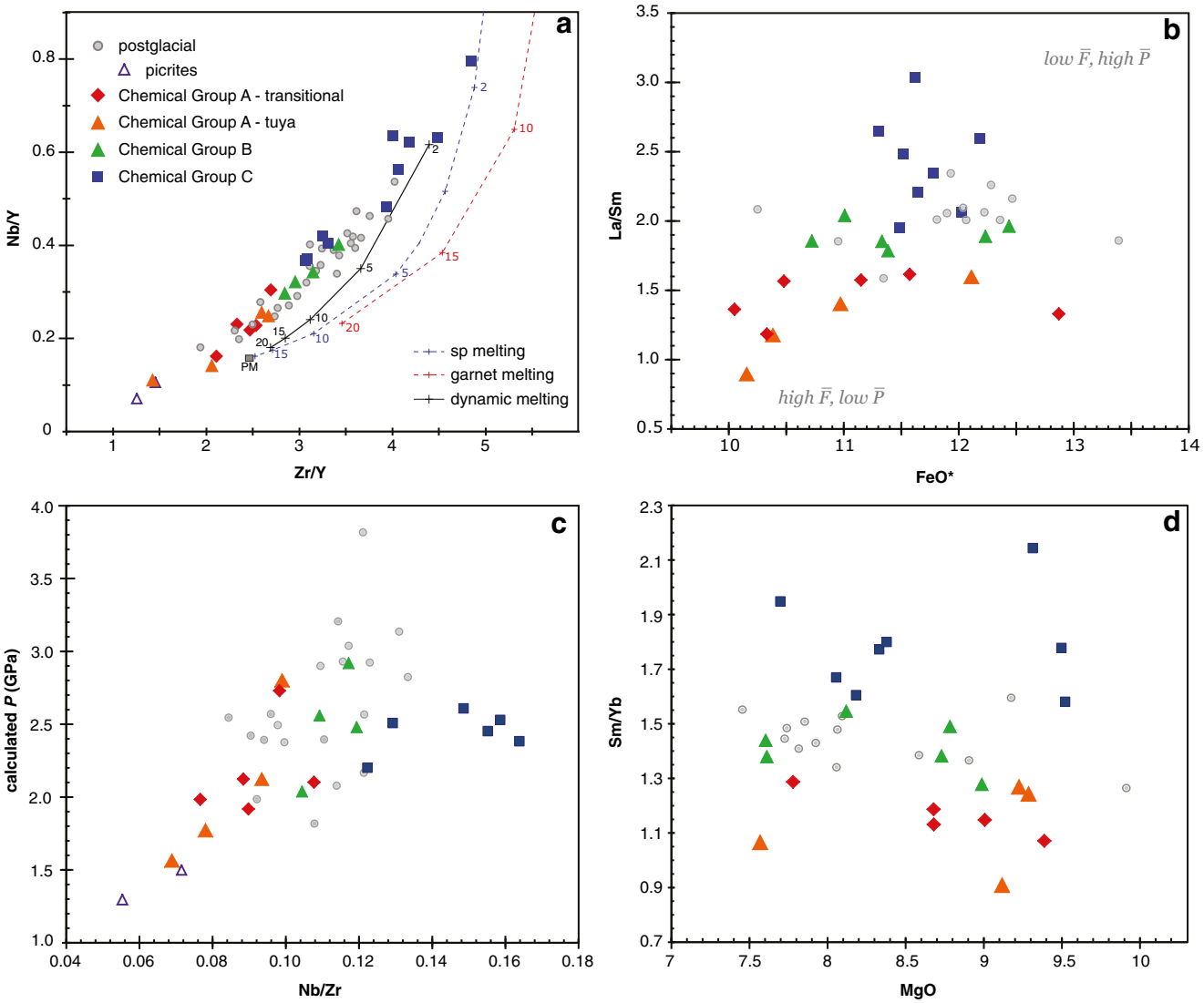

Fig. 8 **a** Nb/Y versus Zr/Y and **b** La/Sm versus FeO* for tuya, transitional, and postglacial samples from the WVZ (data from this study and Sinton et al. 2005). Values plotted are unit averages with symbols denoting their chemical group. Also shown are nonmodal, accumulated fractional melting trends for spinel and garnet peridotite and the dynamic melting trend (assuming 1 % retained melt) from Sinton et al. (2005). Primitive mantle composition of McDonough and Sun (1995) plots within the box designated PM and is used as the source composition for all melting calculations. **c** Mean pressure of mantle melting (*P*) for each unit calculated using the thermobarometer of Lee et al. (2009) plotted against Nb/Zr. *P* values are averaged for each unit using samples with MgO >8.5 wt%. The correlation of calculated melting P with Nb/Zr at low values indicates that the most chemically depleted samples form from melting in the shallowest part of the mantle upwelling zone. **d** Sm/Yb versus MgO, showing that Sm/Yb ratios are relatively insensitive to the amount of differentiation within groups, such as what might occur during storage in the crust. Differences between groups must be controlled by variation in melting processes

deglaciation (Maclennan et al. 2002). Additionally, Stracke et al. (2003) showed striking correlations among incompatible element depletions, decreasing FeO, and less radiogenic isotope ratios among Theistareykir lavas. The correlation of La/Sm with FeO in the present study is consistent with greater incompatible element depletions in the shallowest part of the mantle melting zone. While we do not examine WVZ isotopic data in this current study, Sims et al. (2013) report isotopic data from Theistareykir and Krafla in the NVZ and find that units that erupted shortly after deglaciation preferentially sample the more isotopically depleted mantle component. This is consistent with the largest increase in mantle melting rates occurring in the shallow part of the melting region, where prior melting at depth has already depleted the more fusible enriched component.

To further illustrate this effect, we used the thermobarometer for mafic magmas of Lee et al. (2009) to calculate an estimated average pressure of mantle melting (*P*). Based primarily on magma Si and Mg contents, this thermobarometer is designed to be less sensitive to variations in mantle source composition than the ones based on elements that behave more incompatibly during mantle melting. The thermobarometer is

meant for magmas that have fractionated olivine only, so we apply it here to WVZ samples with MgO ≥8.5 wt % to minimize the effects of plagioclase fractionation. Results are shown in Fig. 8c, with calculated *P* plotted against Nb/Zr. Chemical Group A (average of 2.1 GPa) and the two picrite units (1.4 GPa) have the lowest calculated pressures, while Chemical Groups B and C have more moderate calculated pressures, both averaging ~2.5 GPa. Postglacial lavas yield more variable mean pressures, averaging ~2.6 GPa. The extreme trace element depletions and low calculated melting pressures of Chemical Group A subglacial units (Þórisjökull, Eiríksjökull, and to a lesser degree Krákur) are consistent with the predicted effects from deglaciation-induced decompression melting.

Postglacial Icelandic picrites

The most extreme incompatible element depletions are shown by small picrite lava shields in the WVZ (Fig. 8). Similar small-volume picritic lava shields exist in the Reykjanes Peninsula (Jakobsson et al. 1978; Gee et al. 1998; Sæmundsson et al. 2010) and Northern Volcanic Zone (e.g., Maclennan et al. 2002). Isotopic data on picrites in Iceland require a relatively unradiogenic mantle source (e.g., Elliot et al. 1991; Chauvel and Hémond 2000; Momme et al. 2003; Brandon et al. 2007; Peate et al. 2008), and there has been considerable debate about whether this depleted source is regional ambient MORB mantle or an intrinsic component of the upwelling plume (e.g., Kerr et al. 1995; Fitton et al. 1997, 2003; Chauvel and Hémond 2000; Kempton et al. 2000; Stracke et al. 2003; Thirlwall et al. 2004; Kokfelt et al. 2006; Peate et al. 2008; Koorneef et al. 2012).

Although few have been dated, each of these units appears to be among the oldest postglacial units in its immediate vicinity and most are thought to be early postglacial in age. The three picritic lava shields in the WVZ (Ásar, Búrfell, and Hlíðarhraun) are found in the southernmost end of the neovolcanic zone and are all small in volume (<0.1–0.2 km^3). They are clearly older than the 5200-year-old Leitahraun (Sinton et al. 2005) and likely older than Heiðin há (Jónsson 1978; Sæmundsson et al. 2010). Where exposed, the base of Búrfell lies directly on interglacial shield lavas without an intervening layer of soil (Sinton et al. 2005). Although all are olivine-phyric, olivine accumulation alone cannot account for their extreme incompatible element and isotopic depletions.

The relations shown in Fig. 8 indicate that the depletion in Icelandic picrites can be considered an extension of the trends

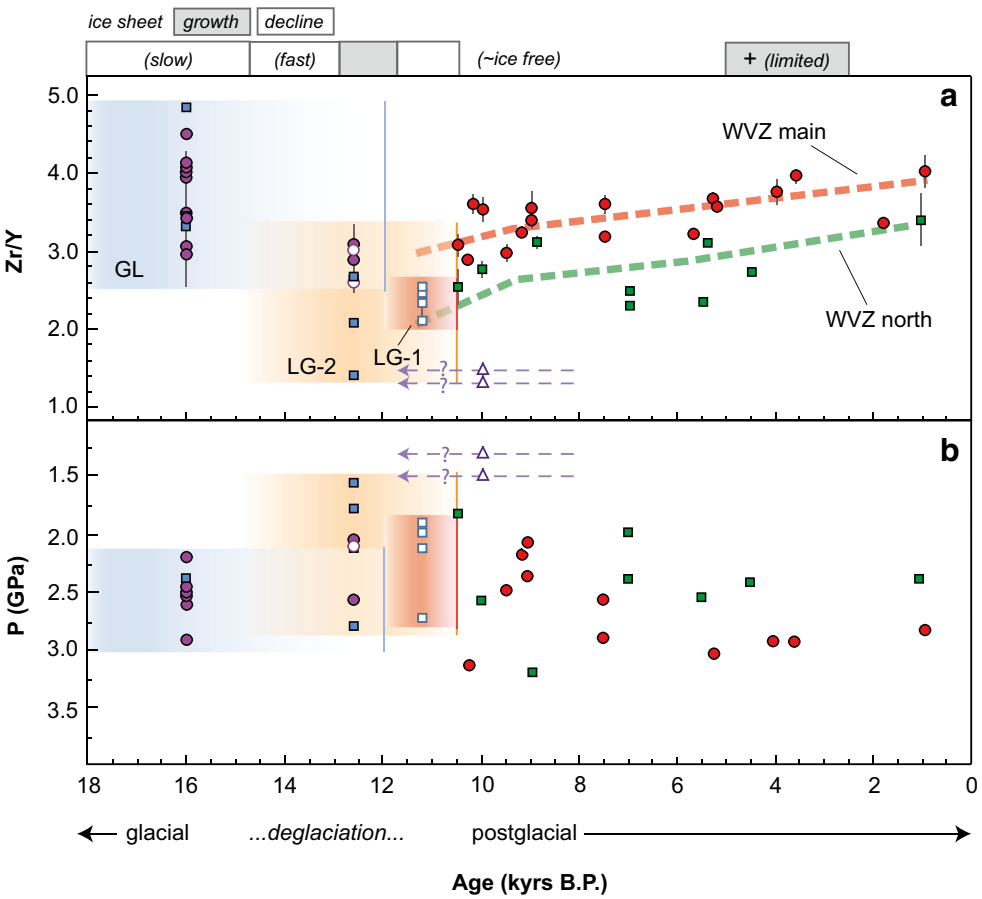

Fig. 9 Variations in **a** Zr/Y and **b** calculated mean mantle melting *P* versus time. Postglacial data (*red*, *green symbols*) and chronology modified from Sinton et al. (2005). *GL* glacial samples likely older than 14.5 Ma; *LG-1* and *LG-2* late Glacial 1 and 2 edifices, respectively. See text for discussion of age constraints and interpretations of glacial units (*purple*, *blue symbols*). *Open symbols* denote transitional units. Top label denotes periods of ice sheet growth (*gray*) and decline (*white*). The greatest incompatible element depletions occur during and immediately following deglaciation. Northern units (*squares*) tend to have lower Zr/Y at the same time as those farther south, a gradient in mantle composition that is thought to be a long-lived feature of the WVZ

produced by deglaciation. Whatever the origin of the depleted component, it should be preferentially sampled by melting in the uppermost mantle, as more enriched mantle components are melted out at greater depths (as discussed above). Previous authors (Fitton et al. 1997, 2003; Momme et al. 2003; Sinton et al. 2005) proposed that continued melting of progressively depleted upwelling mantle (e.g., dynamic melting of Langmuir et al. 1977) can yield the observed trace element compositions of Icelandic picrites. Here we argue that glacial unloading, which preferentially samples the shallowest and most depleted mantle component, provides a realistic physical mechanism for when and why this process might take place.

Late glacial volcanism in the WVZ

The subglacial units in Chemical Group A (Þórisjökull, Eiríksjökull, and to a lesser degree Krákur and Kjalfell) are characterized by strong incompatible element depletions. Their major element compositions yield some of the lowest calculated melting pressures in all the WVZ (Figs. 8 and 9), while their lava surfaces are among the least modified (best preserved) of any of the tuyas in this study. Although variable, passage zone heights for edifices from this group tend to be low, even in the northern highlands (Fig. 7).

These relations illustrate a striking result of this study, which is the extent to which major element composition, incompatible element depletion, passage zone heights, and lava surface preservation covary. The least modified lava surfaces tend to occur in tuyas showing the most profound geochemical signatures of enhanced decompression melting, and most of these features also have the thinnest subaqueous sequences. Considering the potential effect of local climatic conditions on lava surface erosion rates, it is perhaps surprising that these observations correlate as well as they do. Our new data combined with that of Licciardi et al. (2007) indicate that minimum ages from exposure dating can deviate from actual eruption ages by several thousand years. Nevertheless, there is a crude correlation among these ages and geological and geochemical variations that should be time dependent (Table 1).

We identify 14 units in the WVZ (first 14 listed units in Table 1) for which these internally consistent relationships indicate formation after the breakup of the LGM ice sheet. These units include all of the transitional units, as well as those tuyas that exhibit little to no surface modification. Using constraints from glacial chronology, we further subdivide these late glacial units into two groups with different age constraints as follows.

One late glacial group (Late Glacial 1, LG-1) consists of transitional units in the north that likely formed after the advance of the Younger Dryas ice sheet. Kjartansson (1959, 1961) interpreted the morphology of the transitional unit Leggjabrjótur to reflect eruption through thin ice or shallow lake water, followed by prolonged subaerial extrusion of "postglacial" shield lava. Sinton et al. (2005) extended this interpretation to explain similar morphology in other transitional units in the northern WVZ near Langjökull (N. Langjökull, Jökulstallar, and the Hagafell shield). None of these transitional units erupted through an ice sheet sufficiently thick or extensive enough to build the classic table mountain morphology. Each contains subaqueous sections of pillow lava, breccia, and/or hyaloclastite, but only up to ~160 m thick. The lava surfaces of these units (all Surface Category I) are indistinguishable from postglacial lava surfaces, with intact ropes and other delicate surface features, and previous authors (Kjartansson 1983; Sinton et al. 2005) argued that none of them experienced modification by ice after they formed. The subaerial summit crater of Leggjabrjótur (Sólkatla) remains unmodified although the eruptive centers of the others in this group are now buried beneath Langjökull.

The northern part of the WVZ likely retained an extensive ice cover until the end of the Younger Dryas, and these transitional units experienced limited interaction with thin ice or water and show no signs of subsequent modification by overlying glaciers. These relations are consistent with formation during the final stages of melting of the Younger Dryas ice sheet (~11.7–10.5 ka). This period of late glacial activity was only slightly earlier than some of the oldest radiocarbon-dated postglacial lavas, including Hellisheiði A (10,300 years B.P.) and Þingvallahraun (10,200 years B.P.), located further south (Sæmundsson 1991; Sinton et al. 2005 and references therein). It is reasonable to assume that contemporaneous eruptions could have produced subglacial or transitional units in the northern highland area while postglacial units were being emplaced in the more temperate south.

We define a second group (Late Glacial 2, LG-2) that includes both the transitional units in the southern lowlands (Bitra, Hestfjall, Trölladalur, and Heiðin há) and northern tuyas that exhibit little to no surface modification (Surface Categories I–II). The tuyas in this group (Þórisjökull, Eiríksjökull, Krákur, Kjalfell, Hlöðufell, and Skriða) have subaqueous zone thicknesses ranging from ~200 to 540 m. Although some of the northern tuyas have subaerial lava surfaces that look as unmodified as postglacial units, their thick subaqueous sections indicate that these units erupted through a substantial ice sheet. If the estimates for a relatively small Younger Dryas ice sheet are correct, the larger tuyas would have had to have erupted through the LGM ice sheet. The presence of delicate lava features and the general lack of evidence for glacial reworking suggest that any post-formation burial by snow and ice was insufficient to significantly affect lava surfaces.

Some of the LG-2 table mountains (Þórisjökull, Eiríksjökull, and to a lesser degree Krákur) have the most pronounced geochemical signatures predicted for deglaciation-induced mantle decompression (extreme

incompatible trace element depletions (Figs. 4 and 8), coupled to the lowest calculated melting pressures (Fig. 8), and the least modified surfaces of any of the tuyas in this study. This is an important result as it establishes that the geochemical effects of deglaciation became manifest prior to the disappearance of glaciers in Iceland. Maximum absolute ages are difficult to place on these units, but the combined evidence strongly suggests that they erupted near the end of deglaciation, during or just after the bulk of the glacial unloading (after ~14.7 ka) and before the ice sheet had completely melted.

Among the late glacial lava units in the southern lowlands, Trölladalur shows minimal interaction with snow or ice and only on its northern perimeter, and Heiðin há is stratigraphically younger than some early postglacial lavas. Given the relatively unmodified surface of this latter unit, our new exposure age of 9.3±0.4 ka is likely close to its eruption age. Variations in local climate coupled to uncertainties in the thickness of the Younger Dryas ice sheet precludes assignment of individuals in this group to specific ages, but all the LG-2 units likely formed in late glacial to early postglacial time. To accommodate these overlapping age relations and account for uncertainties in ice sheet thickness and glacial retreat chronology, we use the end of deglaciation (~10.5 ka) as a conservative estimate for the minimum age of this group. The generous age range assigned to LG-2 (~14.7–10.5 ka) encompasses most of the major deglaciation.

Other subglacial (glacial, GL) units in the WVZ appear to be older, exhibiting more extensively modified lava surfaces and having the greatest passage zone heights. These units have lost their outermost surfaces (2–3 cm or more in places), and many of them exhibit evidence of glacial scouring, polishing, or significant fracturing. These are units in Surface Categories III and IV whose maximum passage zone heights also tend to be higher (average ~450 m, with a maximum of ~600 m for Hrútfell). We interpret this group as being at least 12 kyrs old, predating the Younger Dryas, and most likely erupting before or during the first major ice retreat, i.e., before ~14.5 ka. Some of the most modified units (e.g., Fanntófell) could even predate the Weichselian. Because of the lack of original lava surfaces and extensive surface modification, "exposure" ages on these features yield values substantially younger than the actual age of formation (Licciardi et al. 2007). Of the five with exposure ages, at least two of them (Högnhöfði and Stóra-Björnsfell) yielded Holocene exposure ages that are clearly too young.

Although we are unable to assign specific ages to individual units, we emphasize that consistency among the various observations is likely to have relative age significance. The maximum passage zone height for individual units tends to be highest in the oldest age group and decreases over time to the transitional units, which record a minimum of possible water/ice interaction, limited both spatially and in thickness. This is broadly consistent with these features erupting through a thinning ice sheet, allowing for local variations in climatic and seasonal effects, and the irregular relationship between glacial thicknesses and ponded water levels. Also, as noted previously, hyaloclastites likely part of Þórisjökull (LG-2, Surface Category I) lap onto the flanks of Geitlandsjökull (GL, Surface Category III) (Fig. 2f), providing additional geological support for these relative age groupings where we have an observable contact between subglacial edifices.

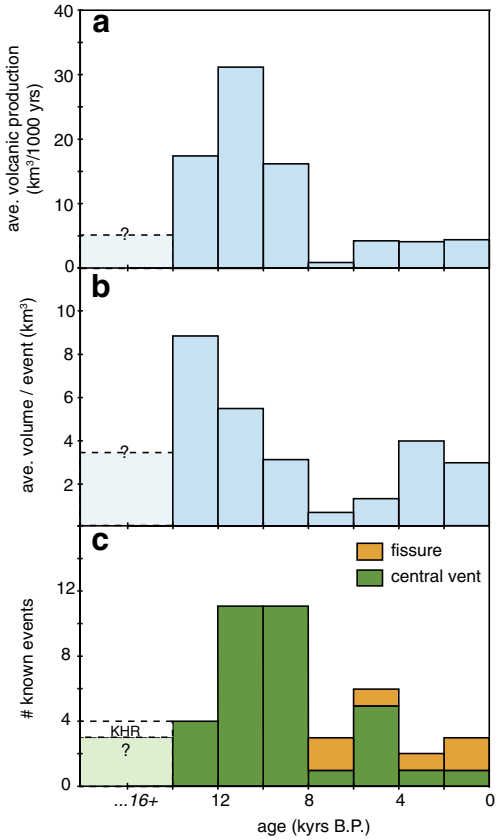

Fig. 10 **a** Average estimated WVZ volcanic production rates (in km^3/1000 years) versus time. See text for description of tuya volume estimates; postglacial and transitional estimates after Sinton et al. (2005). Eruptions are binned in 2000-year increments except for the >14 ka bin for which the maximum unit ages are unknown. The age range for LG-2 spans multiple bins, so volumes have been partitioned between bins proportionally. **b** Average volume per event versus time, using same binning as in **a.** **c** Number of known eruptive units within 2000-year bins, with fissure eruptions shown in *orange* and central vent eruptions (tuyas or postglacial lava shields) in *green*. *KHR* Kálfstindar-Högnhöfði-Rauðafell lineament, which likely began as a 10-km-long fissure that localized to more than one tuya edifice (see text). Note that these plots are likely to reflect undersampling of older and smaller units

Volcanic production and spatiotemporal variations

Although previous studies documented the effects of deglaciation-induced melting in early postglacial lavas (e.g., Jakobsson et al. 1978; Sæmundsson 1991; Gee et al. 1998; Slater et al. 1998; Maclennan et al. 2002; Sinton et al. 2005), our results indicate that the strong geochemical signature of enhanced decompression melting began in the late glacial

period, with the most pronounced geochemical signature of glacial unloading beginning prior to the end of deglaciation (Fig. 9). Abnormally high volcanic production rates persisted into the early Holocene, but the presence of unusually large table mountains in the late glacial WVZ record suggests that surface volcanic production might also have peaked prior to the onset of the postglacial period. Understanding the relationship between geochemical signatures of mantle melting and surface volcanic production has implications for melt migration rates in the mantle and the crust (Maclennan et al. 2002).

To better assess time-varying volcanic production, we divided available unit data (volumes and number of eruptions) into 2000-year bins; volumes for LG-2 units, whose age range spans multiple bins, have been distributed proportionately (Fig. 10). We have few constraints on ages within the GL group. The important point from Fig. 10 is that, even generously apportioning the GL volume to only the last ~6000 years of the glacial period, the data indicate a very large increase in eruptive productivity during deglaciation. Within uncertainties, the analysis suggests volcanic production peaked ~10–14 ka and remained high during the early postglacial period, dropping off dramatically at around ~8 ka. The volcanic production peak (Fig. 10) and profound signature of enhanced decompression melting (Fig. 9) are roughly coincident within the uncertainties for each. An important result of this study is that the volcanic response to deglaciation is evident on the surface before the ice has finished melting and unloading is complete. The presence of numerous (and sometimes very large) table mountains in other neovolcanic zones of Iceland shows that large subglacial outpourings are not limited to the WVZ, but comparable temporal constraints do not presently exist for these areas.

There is also a spatial variation in eruptive volume, with the largest subglacial units located in the northern part of the WVZ (Fig. 2b). Because the effects of glacial unloading should be greatest near the center of Iceland where the ice sheet was thickest, the larger total volume of erupted material in the north is consistent with predictions for deglaciation-induced melting. Additionally, ratios of highly incompatible to less incompatible trace elements tend to be lower in the northern half of the WVZ near Langjökull (Fig. 9), which appears to be a long-lived feature of the WVZ (Schilling et al. 1982; Jakobsson et al. 2000; Sinton et al. 2005). Thus, in this region, variations in the melting process (e.g., higher extents of melting in the north) might be superimposed on a regional gradient in mantle source composition along-axis.

This study includes all of the larger tuyas in the WVZ, which account for the majority of total eruptive volume during this time period, although it is still an incomplete accounting of volcanic activity. It does not include Skriðufell (~8 km^3) or most hyaloclastite ridges of the WVZ. We estimate that the total volume of hyaloclastite ridges and other subglacial features not included in Table 1 amounts to less than ~30 km^3, although it is presently impossible to partition this volume to specific periods within the Pleistocene. There is likely also a component of the total erupted volume that is missing due to burial and erosion of older units, including removal of material during large flooding events (e.g., jökulhlaups). Although this study likely underestimates the total volumes and maximum production rates during deglaciation, the minimum eruptive volumes and corresponding eruption rate estimates comprise the currently best-constrained eruptive chronology of any volcanic zone in Iceland for this time period.

While eruption rates decrease to steady-state values within a few thousand years, the gradual increase in incompatible elements throughout the postglacial period (Fig. 9) indicates that the compositional consequences of deglaciation are longer lived. One might expect trace element compositions to have a more protracted recovery than the melt flux, because chemical transport rates in the mantle should be slower than melt transport rates in the case of porous flow, with the effective velocity for a given trace element inversely proportional to its partition coefficient (e.g., Richter 1986; Navon and Stolper 1987; Spiegelman 1996). In addition, the surface expression of the geochemical signature of glacial unloading could be prolonged by magma mixing and storage in crustal reservoirs.

Crustal processes

Rapid rebound during glacial unloading can lead to fluctuations in local stress regimes and tensile strength of the crust, which could promote eruption and reduce the amount of time magma resides in crustal reservoirs (Gudmundsson 1986). Reduced magma residence time limits the opportunity for magma mixing, assimilation, and evolution, which Gee et al. (1998) argued could account for some of the chemical variations characteristic of early postglacial activity. High and variable MgO contents in the late glacial to early postglacial could be interpreted as reflecting shorter crustal residence times during glacioisostatic rebound (Gudmundsson 1986; Gee et al. 1998), as might be expected from the increased flux of material into the crust during this time. However, processes in the crust alone cannot account for the large variations in incompatible element ratios that are relatively insensitive to crystallization and crustal assimilation (e.g., Sm/Yb, Zr/Y) (Figs. 8d and S1).

Irrespective of stress changes associated with glacial rebound, the dramatic increase in melt supply from deglaciation-induced mantle melting should increase the magma flux through crustal reservoirs and decrease magma residence times. We note that both the estimated frequency of eruption and the average erupted volume for individual events appear to be roughly three times higher during unloading compared to that of the most recent 4000 years (Fig. 10), although such plots reflect undersampling of older and smaller units. Nevertheless, the increase in eruptive productivity seems to be accommodated by both an increase in the number of eruptions

and in the volume of individual eruptive events. Understanding exactly how the excess magma in the crust is being partitioned will require better age constraints than currently available.

Ice retreat and the resulting glacial rebound also appear to be associated with a change in eruptive style. Lava shields are the dominant eruptive style in the WVZ during the early postglacial period (Sinton et al. 2005), and the presence of abundant early postglacial lava shields elsewhere in Iceland also has been associated with glacial rebound (e.g., Sigvaldason et al. 1992; Jakobsson et al. 1978). Gudmundsson (1986) proposed that the bending stresses in the crust associated with rapid isostatic adjustment would promote lava shield formation by decreasing the reservoir volume required to supply a sustained shield eruption. We note that the high melt supply during this period might also promote shield growth. Lava shields, which tend to be large volume and form at relatively low effusion rates, are thought to be sustained by mantle recharge over the course of their long-lived eruptions (Sinton et al. 2005). This is consistent with the tendency for these units to have higher MgO contents (due to lower magma residence times) and with a large volume of recharge melt available during and immediately after glacial unloading to sustain long-lived eruptions. Although we are unable to quantify the relative proportion of central vent versus fissure style eruptions during the late glacial period without knowing the ages of hyaloclastite ridges, we note that every known early postglacial eruption (older than ~8 ka) in the WVZ is a lava shield, while most of the eruptions in the last 4000 years were fissure eruptions (Fig. 10).

There are competing ideas as to whether stress changes in the crust during glacioisostatic rebound promote or inhibit eruption, and the effects likely vary depending on location with respect to the center of the ice sheet (e.g., Pagli and Sigmundssson 2008; Albino et al. 2010; Sigmundsson et al. 2010; Hooper et al. 2011). Glacial unloading should reduce the confining lithostatic stress, which may decrease the amount of overpressure required to initiate diking (e.g., McLeod and Tait 1999; Jellinek and DePaolo 2003; Jellinek et al. 2004). However, Hooper et al. (2011) suggest that pressure changes associated with ice retreat may also alter the magma storage capacity of the crust, favoring intrusion over extrusion depending on dike orientation and proximity to the edge of the ice sheet. They suggest that, at least in the present-day Upptyppingar region (Northern Volcanic Zone), the overall effect is to increase the expected erupted volume beneath the melting ice cap for dikes oriented parallel to the rift zone. This relationship could help explain the formation of such large volume table mountains during deglaciation.

Conclusions

Tuyas and other subglacial eruptions represent a significant portion of the volcanic budget in Iceland. Those in the Western Volcanic Zone have eruptive volumes up to ~48 km^3 but still appear to be monogenetic. Water-magma interactions during eruption result in a range of lithological facies and exhibit evidence for fluctuating lake levels during eruption. Some units record multiple or dipping subaqueous to subaerial transition zones. We have documented two cases of subglacial eruptions that likely began as 5–10-km-long subglacial fissure eruptions that later localized to point sources, eventually constructing subaerial table mountains.

WVZ subglacial edifices show a range of morphologies and internal constitution. Some units, which we call "transitional," have relatively thin (mostly <160 m), locally occurring subaqueous sections. Tuyas with the classic steep-sided table mountain morphology have thick subaqueous sections up to ~600 m high. Subaerial lava surfaces on transitional units are relatively unmodified by post-emplacement erosion, similar to the surfaces of older postglacial lavas. Pristine lava surfaces also were observed on some larger tuyas, most notably on Þórisjökull, although most tuyas with large passage zone heights tend to have more extensively modified lava surfaces.

Lava and hyaloclastite samples from WVZ subglacial and transitional units encompass the compositional range of WVZ postglacial lavas and significantly extend the compositional range of the most highly incompatible trace elements. Particularly notable are a subset of subglacial and transitional units that are strongly depleted in incompatible elements and have low FeO and slightly higher than average SiO_2 and CaO contents. These compositional characteristics are shared by some very early postglacial lavas in the WVZ and elsewhere in Iceland. This geochemical signature is consistent with increased decompression melting preferentially in the shallow mantle in response to glacial unloading.

We combine field relations, observations of lava surface preservation, constraints from passage zone heights, and minimum ages from cosmogenic ^3He exposure dating to distinguish late-glacial volcanic edifices from older ones. Older tuyas tend to have high passage zone heights indicating eruption through thick ice, and heavily modified surfaces, with extensive weathering and local evidence of post-eruption glacial activity, including glacial straie, polished surfaces, and extensive erosion and valley formation. These edifices tend to have chemical compositions similar to, or more enriched in incompatible elements than, WVZ postglacial lavas.

We recognize two younger groups of edifices, both of which we interpret to have formed after the onset of deglaciation (<14.7 ka), when rapidly melting ice sheets increased decompression rates and preferentially increased melting in the shallow, depleted mantle. Both groups have subaerial lava surface morphologies that range from nearly pristine, with ropes and other delicate surface features intact, to moderate degrees of surface modification and removal of the outermost 1–3 cm of lava surfaces. The youngest group includes

transitional units in the northern highlands, which likely overlap in age with the oldest early postglacial lavas in the southern WVZ. Another group of late glacial edifices includes transitional units in the southern lowlands (Bitra, Hestfjall, Trölladalur, and Heiðin há) and larger tuyas that must have erupted through thicker glaciers, but still retain relatively unmodified lava surfaces. These include Þórisjökull and Eiríksjökull which, together with the picrite units Ásar and Búrfell, have lavas with the most profound incompatible element depletions observed in the WVZ.

These new observations suggest a maximum in volcanic production in the WVZ after the onset of deglaciation, but prior to complete ice removal. The timing of this peak in eruptive activity occurs earlier than noted in previous studies based solely on postglacial data. Increased volcanic production continues into the early postglacial period, with average eruption rates remaining high until ~8 ka. Distinctive chemical compositional characteristics coincide with this period of anomalously high productivity. In contrast with the relatively rapid decline in volcanic production, incompatible element concentrations gradually increase back toward steady-state levels throughout the entire postglacial period. The observed geochemical variations during and shortly after deglaciation are consistent with increased melting occurring preferentially in the shallow, depleted upper mantle, as predicted by models of deglaciation-induced mantle decompression. This process can also explain the preferential eruption of highly depleted, high-MgO picritic lavas in early postglacial time.

Acknowledgments We thank Alice Colman, Mark Higley, and JoAnn Sinton for assistance in the field; Eric Hellebrand for the help with the microprobe and XRF analyses; Chuck Fraley for ICP-MS analyses; and JoAnn Sinton for thin section preparation. Many thanks to Joshua Curtice for assistance with the mineral separates and helium measurements and to Logi Karlsson for providing us with an excellent field vehicle. We are grateful to John Maclennan, Joseph Licciardi, editor Thorvaldur Thordarson, and two anonymous reviewers, whose thorough reviews led to substantial improvements in the manuscript. This research was supported by the National Science Foundation grant EAR09-11301. This is SOEST contribution #9299.

References

Albino F, Pinel V, Sigmundsson F (2010) Influence of surface load variations on eruption likelihood: application to two Icelandic subglacial volcanoes, Grímsvötn and Katla. Geophys J Int 181:1510–1524

Brandon AD, Graham DW, Waight TE, Gautason B (2007) ^{186}Os and ^{187}Os enrichments and high-^{3}He/^{4}He sources in the Earth's mantle: evidence from Icelandic picrites. Geochim Cosmochim Acta 71: 4570–4591. doi:10.1016/j.gca.2007.07.015

Chauvel C, Hémond C (2000) Melting of a complete section of recycled oceanic crust: trace element and Pb isotopic evidence from Iceland. Geochem, Geophys, Geosyst 1:1–21. doi:10.1029/1999GC000002

Eason DE, Sinton JM (2009) Lava shields and fissure eruptions of the Western Volcanic Zone, Iceland: evidence for magma chambers and crustal interaction. J Volcanol Geotherm Res 186:331–348. doi:10.1016/j.jvolgeores.2009.06.009

Edwards BR, Skilling IP, Cameron B, Haynes C, Lloyd A, Hungerford JHD (2009) Evolution of an englacial volcanic ridge: Pillow Ridge tindar, Mount Edziza volcanic complex, NCVP, British Columbia, Canada. J Volcanol Geotherm Res 185:251–275

Elliot TR, Hawkesworth CJ, Grönvold K (1991) Dynamic melting of the Iceland plume. Nature 351:201–206. doi:10.1038/351201a0

Fitton JG, Saunders AD, Norry MJ, Hardarson BS, Taylor RN (1997) Thermal and chemical signature of the Iceland plume. Earth Planet Sci Lett 153:197–208. doi:10.1016/S0012-821X(97)00170-2

Fitton JG, Saunders AD, Kempton PD, Hardarson BS (2003) Does depleted mantle form an intrinsic part of the Iceland plume? Geochem, Geophys, Geosyst 4(3):1032. doi:10.1029/2002GC0000424

Flowers GE, Björnsson H, Geirsdóttir Á, Miller GH, Black JL, Clarke GKC (2008) Holocene climate conditions and glacier variation in central Iceland from physical modelling and empirical evidence. Quat Sci Rev 27:797–813

Gee MAM, Taylor RN, Thirlwall MT, Murton BJ (1998) Glacioisostacy controls chemical and isotopic characteristics of tholeiites from the Reykjanes Peninsula, SW Iceland. Earth Planet Sci Lett 164:1–5

Geirsdóttir Á, Eiríksson J (1994) Sedimentary facies and environmental history of the Late-glacial glaciomarine Fossvogur sediments in Reykjavík, Iceland. Boreas 23:164–176

Geirsdóttir Á, Hardardóttir J, Sveinbjörnsdóttir ÁE (2000) Glacial extent and catastrophic meltwater events during the deglaciation of Southern Iceland. Quat Sci Rev 19:1749–1761

Geirsdóttir Á, Miller GH, Andrews JT (2007) Glaciation, erosion, and landscape evolution of Iceland. Holocene and latest Pleistocene climate and glacier fluctuations in Iceland. J Geodynamics 43:170–186

Geirsdóttir Á, Miller GH, Axford Y, Ólafsdóttir S (2009) Holocene and latest Pleistocene climate and glacier fluctuations in Iceland. Quat Sci Rev 28:2107–2118

Goodfellow BW (2007) Relict non-glacial surfaces in formerly glaciated landscapes. Earth-Sci Rev 80:47–73

Gosse JC, Phillips FM (2001) Terrestrial in situ cosmogenic nuclides: theory and application. Quat Sci Rev 20:1475–1560

Gudmundsson A (1986) Mechanical aspects of postglacial volcanism and tectonics of the Reykjanes Peninsula, Southwest Iceland. J Geophys Res 91:12,711–12,721

Guðmundsson HJ (1998) Holocene glacier fluctuations of the Eiríksjökull ice cap, west central Iceland. Jökull 46:17–28

Gudmundsson MT, Sigmundsson F, Björnsson H, Högnadóttir T (2004) The 1996 eruption at Gjálp, Vatnajökull ice cap, Iceland: efficiency of heat transfer, ice deformation and subglacial water pressure. Bull Volc 66:46–65

Hardarson BS, Fitton JG (1991) Increased mantle melting beneath Snaefellsjökull volcano during late Pleistocene deglaciation. Nature 353:62–64

Harris AJL, Murray JB, Aries SE, Davies MA, Flynn LP, Wooster MJ, Wright R, Rothery DA (2001) Effusion rate trends at Etna and Krafla and their implications for eruptive mechanisms. J Volcanol Geotherm Res 102:237–270

Hirose K, Kushiro I (1993) Partial melting of dry peridotites at high pressures: determination of compositions of melts segregated from peridotite using aggregates of diamond. Earth Planet Sci Lett 114: 477–489

Hirschmann MM, Ghiorso MS, Stolper EM (1999) Calculation of peridotite partial melting from thermodynamic models of minerals and melts. II. Isobaric variations in melts near the solidus and owing to variable source composition. J Petrol 40:297–313

Hooper A, Ófeigsson B, Sigmundsson F, Lund B, Einarsson P, Geirsson H, Sturkell E (2011) Increased capture of magma in the crust promoted by ice-cap retreat in Iceland. Nat Geosci 4:783–786. doi:10.1038/NGEO1269

Hubbard A, Sugden J, Dugmore A, Norðdahl H, Pétursson HG (2006) A modelling insight into the Icelandic Late Glacial Maximum ice sheet. Quat Sci Rev 25:2283–2296

Jakobsson SP, Gudmundsson MT (2008) Subglacial and intraglacial volcanic features in Iceland. Jökull 58:179–196

Jakobsson SP, Johnson GL (2012) Intraglacial volcanism in the Western Volcanic Zone, Iceland. Bull Volcanol 74:1141–1160. doi:10.1007/s00445-012-0589-x

Jakobsson SP, Jónsson J, Shido F (1978) Petrology of the western Reykjanes Peninsula, Iceland. J Petrol 19:669–705

Jakobsson SP, Johnson GL, Moore JG (2000) A structural and geochemical study of the Western Volcanic Zone, Iceland: preliminary results. InterRidgeNews 9:27–33

Jaques A, Green D (1979) Determination of liquid compositions in high-pressure melting of peridotite. Amer Mineral 64:1312–1321

Jellinek AM, DePaolo DJ (2003) A model for the origin of large silicic magma chambers: precursors of catastrophic caldera-forming eruptions. Bull Volcanol 65:363–381

Jellinek AM, Manga M, Saar MO (2004) Did melting glaciers cause volcanic eruptions in eastern California? Probing the mechanics of dike formation. J Geophys Res 109:B09206. doi:10.1029/2004JB002978

Jóhannesson H, Sæmundsson K (1998) Geologic map of Iceland, 1:500, 000. Bedrock Geology 2nd ed. Icelandic Inst of Nat Hist, Reykjavík

Jones JG (1969) Intraglacial volcanoes of the Laugarvatn region, southwest Iceland, I. Quart J Geol Soc London 124:197–211

Jones JG (1970) Intraglacial volcanoes of the Laugarvatn region, southwest Iceland, II. J Geol 78:127–140

Jónsson J (1978) Geology of Reykjanes. Orkustofnun Jarðhitadeild 7831, 303 pp., Reykjavík

Jull M, McKenzie D (1996) The effect of deglaciation on mantle melting beneath Iceland. J Geophys Res 101:21,815–21,828

Kempton PD, Fitton JG, Saunders AD, Nowell GM, Taylor RN, Hardarson BS, Pearson G (2000) The Iceland plume in space and time: a Sr-Nd-Pb-Hf study of the North Atlantic rifted margin. Earth Planet Sci Lett 177:255–271. doi:10.1016/S0012-821X(00)00047-9

Kerr AC, Saunders AD, Tarney J, Berry NB, Hards VL (1995) Depleted mantle plume geochemical signature: no paradox for plume theories. Geology 23:843–846

Kjartansson G (1959) The Móberg formation. In: Thorarinsson S, Einarsson T, and Kjartansson G. On the geology and geomorphology of Iceland. Geografiska Annaler 41:135-69

Kjartansson G (1961) Glefsur um jarðfræði (Notes on geology). In: Árbók Ferðafélags Íslands, Reykjavík, pp 17–29

Kokfelt TF, Hoernle K, Hauff F, Fiebig J, Werner R, Garbe-Schönberg D (2006) Combined trace element and Pb-Nd-Sr-O isotope evidence for recycled oceanic crust (upper and lower) in the Iceland mantle plume. J Petrol 47:1705–1749. doi:10.1093/petrology/eg1025

Koorneef JM, Stracke A, Bourdon B, Meier MA, Jochum KP, Stoll B, Grönvold K (2012) Melting of a two-component source beneath Iceland. J Petrol 53:127–157

Kurz MD (1986) In situ production of terrestrial cosmogenic helium and some applications to geochronology. Geochim Cosmochim Acta 50: 2855–2862

Kurz MD, Colodner D, Trull TW, Moore RB, O'Brien K (1990) Cosmic ray exposure dating with in situ produced cosmogenic ^{3}He results from young Hawaiian lava flows. Earth Planet Sci Lett 97:177–189

Kushiro I (1996) Partial melting of a fertile mantle peridotite at high pressures: an experimental study using aggregates of diamond. Geophys Monograph 95:109–122, AGU, Washington DC

Langmuir CH, Bender JF, Bence AE, Hanson GN, Taylor SR (1977) Petrogenesis of basalts from the FAMOUS area, Mid-Atlantic Ridge. Earth Planet Sci Lett 36:133–156

Larsen DJ, Miller GH, Geirsdóttir Á, Ólafsdóttir S (2012) Non-linear Holocene climate evolution in the North Atlantic: a high-resolution, multi-proxy record of glacial activity and environmental change from Hvítárvatn, central Iceland. Quat Sci Rev 39:14–25

Le Breton E, Dauteuil O, Biessy G (2010) Post-glacial rebound of Iceland during the Holocene. J Geol Soc London 167:417–432

Lee C-TA, Luffi P, Plank T, Dalton H, Leeman WP (2009) Constraints on the depths and temperatures of basaltic magma generation on Earth and other terrestrial planets using new thermobarometers for mafic magmas. Earth Planet Sci Letts 279:20–33

Licciardi JM, Kurz MD, Clark PU, Brook EJ (1999) Calibration of cosmogenic ^{3}He production rates from Holocene lava flows in Oregon, USA, and effects of the Earth's magnetic field. Earth Planet Sci Lett 172:261–271

Licciardi JM, Kurz MD, Curtice JM (2006) Cosmogenic ^{3}He production rates from Holocene lava flows in Iceland. Earth Planet Sci Lett 246: 251–264

Licciardi JM, Kurz MD, Curtice JM (2007) Glacial and volcanic history of Icelandic table mountains from cosmogenic ^{3}He exposure ages. Quat Sci Rev 26:1529–1546

Maclennan J, Jull M, McKenzie D, Slater L, Grönvold K (2002) The link between volcanism and deglaciation in Iceland. Geochem, Geophys, Geosyst 3:1–25. doi:10.1029/2001GC000282

Maclennan J, McKenzie D, Hilton F (2003) Geochemical variability in a single flow from northern Iceland. J Geophys Res 108:ECV 4-1–ECV 4-21. doi:10.1029/2000JB000142

Mathews WH (1947) "Tuyas", flat-topped volcanoes in northern British Columbia. Am J Sci 245:560–570

McDonough WF, Sun S-S (1995) The composition of the Earth. Chem Geol 120:223–253

McLeod P, Tait S (1999) The growth of dykes from magma chambers. J Volcanol Geotherm Res 92:231–246

Momme P, Óskarsson N, Keays RR (2003) Platinum-group elements in the Icelandic rift system: melting processes and mantle sources beneath Iceland. Chem Geol 196:209–234

Moore JG, Calk LC (1991) Degassing and differentiation in subglacial volcanoes, Iceland. J Volcanol Geotherm Res 46:157–180

Moore JG, Hickson CJ, Calk LC (1995) Tholeiitic-alkalic transition at subglacial volcanoes, Tuya region, British Columbia, Canada. J Geophys Res B12:24,577–24,592

Navon O, Stolper E (1987) Geochemical consequences of melt percolation: the upper mantle as a chromatographic column. J Geol 95:285–307

Norðdahl H, Pétursson HG (2005) Relative sea level changes in Iceland. New aspect of the Weichselian deglaciation of Iceland. In: Caseldine C, Russell A, Harðardóttir J, Knudsen Ó (eds) Iceland—modern processes and past environments. Elsevier, Amsterdam, pp 25–78

Norðdahl H, Ingólfsson Ó, Pétursson HG, Hallsdóttir M (2008) Late Weichselian and Holocene environmental history of Iceland. Jökull 58:343–364

Pagli C, Sigmundssson F (2008) Will present day glacier retreat increase volcanic activity? Stress induced by recent glacier retreat and its effect on magmatism at Vatnajökull ice cap, Iceland. Geophys Res Lett 35:L09304. doi:10.1029/2008GL033510

Peate DW, Baker JA, Jakobsson SP, Waight TE, Kent AJR, Grassineau NV, Skovgaard AC (2008) Historic magmatism on the Reykjanes Peninsula, Iceland: a snap-shot of melt generation at a ridge segment. Contrib Mineral Petrol 157:359–382. doi:10.1007/S00410-008-0339-4

Pederson GBM, Grosse P (2014) Morphometry of subaerial shield volcanoes and glaciovolcanoes from Reykjanes Peninsula, Iceland: effects of eruption environment. J Volcanol Geotherm Res 282:115–133

Pigati JS, Lifton NA (2004) Geomagnetic effects on time-integrated cosmogenic nuclide production with emphasis on in situ ^{14}C and ^{10}Be. Earth Planet Sci Lett 226:193–205

Richter FM (1986) Simple models of trace element fractionation during melt segregation. Earth Planet Sci Lett 77:333–344

Rossi MJ (1996) Morphology and mechanism of eruption of postglacial shield volcanoes in Iceland. Bull Volcanol 57:530–540

Sæmundsson K (1980) Outline of the geology of Iceland. Jökull 29:7–28

Sæmundsson K (1991) Jardfrædi Kröflukerfisins. In: Gardarsson A, Einarsson A (eds) Náttúra Mývatns. Hid islenska náttúrufrædifélg, Reykjavík, pp 24–95

Sæmundsson K (1998) Geology of the Thingvallavatn area. Oikos 64: 40–68

Sæmundsson K, Jóhannesson H, Hjartarson A, Kristinsson SG, Sigurgeirsson MA (2010) Geological map of Southwest Iceland, 1:100 000. Iceland GeoSurvey, Reykjavík

Schilling J-G, Meyer PS, Kingsley RH (1982) Evolution of the Iceland hotspot. Nature 296:313–320

Schmidt P, Lund B, Hieronymus C, Maclennan J, Árnadóttir T, Pagli C (2013) Effects of present-day deglaciation in Iceland on mantle melt production rates. J Geophys Res 118:3366–3379. doi:10.1002/jgrb.50273

Sigmundsson F (1991) Post-glacial rebound and asthenosphere viscosity in Iceland. Geophys Res Lett 18:1131–1134

Sigmundsson F, Pinel V, Lund B, Albino F, Pagli C, Geirsson H, Sturkell E (2010) Climate effects on volcanism: influence on magmatic systems of loading and unloading from ice mass variations, with examples from Iceland. Phil Trans R Soc A 368:2519–2534

Sigvaldason GE, Annertz K, Nilsson M (1992) Effect of glacier loading/deloading on volcanism: postglacial volcanic production rate of the Dyngjufjöll area, central Iceland. Bull Volcanol 54:385–392

Sims KWW, Maclennan J, Blichert-Toft J, Mervine EM, Blusztajn J, Grönvold K (2013) Short length scale mantle heterogeneity beneath Iceland probed by glacial modulation of melting. Earth Planet Sci Lett 379:146–157

Sinton JM, Grönvold K, Sæmundsson K (2005) Postglacial eruptive history of the Western Volcanic Zone, Iceland. Geochem, Geophys, Geosyst 6:Q12009. doi:10.1029/2005GC001021

Skilling IP (2009) Subglacial to emergent basaltic volcanism at Hlöðufell, south-west Iceland: a history of ice-confinement. J Volcanol Geotherm Res 185:276–289

Slater L, Jull M, McKenzie D, Grönvold K (1998) Deglaciation effects on mantle melting under Iceland: results from the northern volcanic zone. Earth Planet Sci Lett 164:151–164

Smellie JL (2000) Subglacial eruptions. In: Sigurdsson H (ed) Encyclopedia of volcanoes. Academic, San Diego, pp 403–418

Smellie JL (2006) The relative importance of supraglacial versus subglacial meltwater escape in basaltic subglacial tuya eruptions: an important unresolved conundrum. Earth-Sci Rev 74: 241–268

Smellie JL, Hole MJ, Nell PAR (1993) Late Miocene valley-confined subglacial volcanism in northern Alexander Island, Antarctic Peninsula. Bull Volcanol 55:273–288

Sobolev AV, Hofmann AW, Nikogosian IK (2000) Recycled oceanic crust observed in 'ghost plagioclase' within the source of Mauna Loa lavas. Nature 404:986–990

Spiegelman M (1996) Geochemical consequences of melt transport in 2-D: the sensitivity of trace elements to mantle dynamics. Earth Planet Sci Lett 139:115–132

Stracke A, Zindler A, Salters VJM, McKenzie D, Blichert-Toft J, Albarède F, Grönvold K (2003) Theistareykir revisited. Geochem, Geophys, Geosyst 4(2):8507. doi:10.1029/2001GC000201

Svensson A, Andersen KK, Bigler M, Clausen HB, Dahl-Jensen D, Davies SM, Johnson SJ, Muscheler R, Parrenin F, Rasmussen SO, Röthlisberger R, Seierstad I, Steffensen JP, Vinther BM (2008) A 60, 000 year Greenland stratigraphic ice core chronology. Clim Past 4: 47–57

Thirlwall MF, Gee MAM, Taylor RN, Murton BJ (2004) Mantle components in Iceland and adjacent ridges investigated using double-spike Pb isotope ratios. Geochim Cosmochim Acta 68:361–386. doi:10.1016/S0016-7037(03)00424-1

Thorarinson S, Steinthorsson S, Einarsson T, Kristannsdottir H, Oskarsson N (1973) The eruption on Heimaey, Iceland. Nature 241:372–375

Vilmundardóttir E, Larsen G (1986) Productivity pattern of the Veidivötn fissure swarm, Southern Iceland, in postglacial times. Preliminary results: paper presented at 17e Nordiska Geologmötet, Helsingsfors Univ, Helsinki, Finland

Wadge G (1981) The variation of magma discharge during basaltic eruptions. J Volc Geotherm Res 11:139–168

Walker GPL (1965) Some aspects of Quaternary volcanism in Iceland. Trans Leicester Lit Phil Soc 59:25–40

Wasylenki LE, Baker MB, Kent AJR, Stolper EM (2003) Near-solidus melting of the shallow upper mantle: partial melting experiments on depleted peridotite. J Petrol 44:1163–1191

Werner R, Schmincke H-U (1999) Englacial vs lacustrine origin of volcanic table mountains: evidence from Iceland. Bull Volcanol 60:335–354